Vibration Response Prediction Methodologies
for
Coupled Structures

by

Hakan UÇAR

A Thesis Submitted to the
Graduate School of Engineering
in Partial Fulfillment of the Requirements for
the Degree of

Doctor of Philosophy
in
Mechanical Engineering

Koc University

July 2015

Koc University

Graduate School of Sciences and Engineering

This is to certify that I have examined this copy of a doctor of philosophy thesis by

Hakan UÇAR

and have found that it is complete and satisfactory in all respects,
and that any and all revisions required by the final
examining committee have been made.

Committee Members:

_____

İpek Başdoğan, Ph. D. (Advisor)

_____

Ahmet Güney, Ph. D.

_____

Demircan Canadinc, Ph. D.

_____

Murat Sozer, Ph. D.

_____

Cüneyt Ezgi, Ph. D.

Date: _____

ABSTRACT

Complex structures are usually composed of various subsystems coupled by several rigid or elastic couplings. Prediction of the vibration response at these complex structures such as aerospace, marine and automotive vehicles is an important engineering issue in terms of design optimization and component selection.

Considering this demand, this dissertation presents the vibration response prediction (VRP) methodologies such as mount stiffness method, transmissibility matrix method, matrix pseudo and direct inversion methods for the structures coupled with rigid and elastic couplings. Among the presented VRP methodologies, most consideration is given to the matrix inversion methods which involve an inverted frequency response function (FRF) matrix and a vector of vibration responses. In accordance with the matrix inversion methods, experimental and numerical case studies are conducted. At first, a rigidly coupled planar structure is considered and VRP methodology based on the matrix pseudo inversion method is applied along with singular value decomposition (SVD). Tikhonov regularization with the cross validation functions is investigated for improving the prediction results. Secondly, direct inversion method is applied for a structure coupled with two rigid links considering the cross-coupling effects. Results of the pseudo and direct inversion methods are compared for the case study presented. Effects of the measurement errors such as mass loading and existing noise on the prediction results are also demonstrated with the same structure.

Finally, the structures connected with the elastic mounts are discussed since vibratory sources are usually connected to the supporting structures via rubber mounts. A hybrid methodology that incorporates the numerical model with the experimental measurement results is proposed to improve the predicted vibration response. In order to perform the hybrid VRP methodology for the rubber linked structure, hyperelastic and viscoelastic behavior of the rubber mounts are included within the numerical model and a simulation

algorithm is developed. Considerations of this method such as the generation of an accurate numeric model and selection of the force identification points are also discussed. Force identification points are selected based on a metric that is composed of average condition number of the FRF matrix across the whole frequency of interest. The effectiveness of the proposed method is demonstrated by comparing the predicted results with the measured vibration responses.

ÖZETÇE

Kompleks yapılar genellikle rijit veya elastik bağlantı elemanları ile birbirlerine bağlanmış birçok alt sistemlerden oluşmaktadır. Otomotiv, hava ve deniz taşıtları gibi kompleks yapılarda titreşim tepkisinin öngörülmesi dizayn optimizasyonu ve ekipman seçimi açısından önemli bir mühendislik konusudur.

Bu gereksinim dikkate alınarak bu tezde rijit ve elastik bağlı yapılar için bağlantı rijitlik metodu, iletilebilirlik matris metodu, matris tersine çevirme metodu gibi titreşim tepki öngörüsü (TTÖ) metotları sunulmuştur. Bahse konu metotlar arasından, en çok matris tersine çevirme metoduna odaklanılmıştır. Matris tersine çevirme metodu, tersi alınan frekans tepki fonksiyonları (FTF) matrisi ve titreşim tepki vektöründen oluşmaktadır. Matris tersine çevirme metoduna ilişkin deneysel ve nümerik çalışmalar yapılmıştır. Öncelikle, rijit bağlı düzlemsel yapılar ele alınmış ve benzetik matris tersine çevirme metodunu içeren TTÖ teknikleri tekil değer ayrışması (TDA) ile birlikte uygulanmıştır. Sonuçları iyileştirmek amacıyla Tikhonov düzenleme teknikleri ile doğrulama fonksiyonlarının etkisi incelenmiştir. İkinci çalışma olarak, doğrudan matris tersine çevirme metodu ve bağıl etkiler dikkate alınarak iki rijit link ile bağlanmış bir yapı üzerinde TTÖ çalışması yapılmıştır. Bu çalışma için, benzetik ve doğrudan matris tersine çevirme metotlarının sonuçları mukayese edilmiştir. Ayrıca, kütle etkisi ve sinyalde gürültü gibi ölçüm hatalarının sonuçlara olan etkisi aynı yapı üzerinden nümerik bir çalışma ile gösterilmiştir.

Son olarak, titreşim kaynakları kaidelerine genellikle lastik sönümleyiciler ile bağlandığından, elastik bağlı yapılar dikkate alınmıştır. Öngörü sonuçlarını iyileştimek amacıyla nümerik ve deneysel verileri entegre eden bir hibrid TTÖ metodu önerilmiştir. Lastik bağlı yapıda hibrid metodu uygulamak için, lastik sönümleyicilerin hiperelastik ve viskoelastik davranışı incelenmiş ve nümerik model ve simulasyon algoritması

sunulmuştur. Doğru bir nümerik modelin oluşturulması ve kuvvet belirleme noktarının seçilmesi gibi konular da ele alınmıştır. Kuvvet belirleme noktaları, FTF matrisinin tüm frekans aralığını içeren ortalama kondüsyon numarasına bağlı bir metrik ile seçilmiştir. Önerilen metodun etkinliği, öngörü ve ölçüm sonuçlarının mukayese edilmesi ile gösterilmiştir.

ACKNOWLEDGEMENT

TABLE OF CONTENTS

LIST OF TABLES

TABLE OF FIGURES

Chapter 1.

INTRODUCTION

Noise, vibration and harshness (NVH) have a vital importance especially for the complex structures composed of several substructures. Vibration has always been an important issue in terms of reliability and quality while noise is essential to the system users and also the environment [1]. Besides, noise and vibration have damaging health effects. It can result in a large number of physiological and psychological disabilities such as hearing loss, fatigue, misunderstanding, decreased working capacity, concentration loss and irritation etc. [2] Thus, it is essential to monitor and control the noise and vibration characteristics of the structures.

A vibro-acoustic system mainly consists of two components; active and passive part, as illustrated in Fig. 1.1. Active part is basically the source which results in vibro-acoustic energy. Two types of sources can be defined; structural and acoustic. Regarding the structural sources, these components, such as engines, pumps or compressors etc., excite the passive subsystem through structural connections. Acoustic sources can be vibrating surfaces producing sound, such as the cylinder cover, and flow induced noise such as exhaust pipes, ventilation fans and air intakes. These sources can be characterized by their source strength, often measured in volume velocity or displacement.

Passive side is composed of the receivers and the paths through which the vibro-acoustic energy is propagated. Paths starting at a structural source are called structure-

borne paths whereas paths starting at an acoustic source are called airborne paths. A representative example for typical transfer paths is illustrated in Fig. 1.2 for an engine installed on the engine room of a ship.

Transfer paths can be analytically expressed as transfer functions or frequency response functions (FRF). These FRFs used for the structure-borne paths are usually measured as receptance, mobility or accelerance. As for the airborne paths, transfer functions are referred to as noise transfer functions (NTF) in order to distinguish them from other FRFs.

Final component of the system is the receiver such as a driver, passenger, a vibration sensitive device or a point which should be monitored. The receivers can be defined by their vibration or acoustic response such as sound pressure or acceleration or displacement.
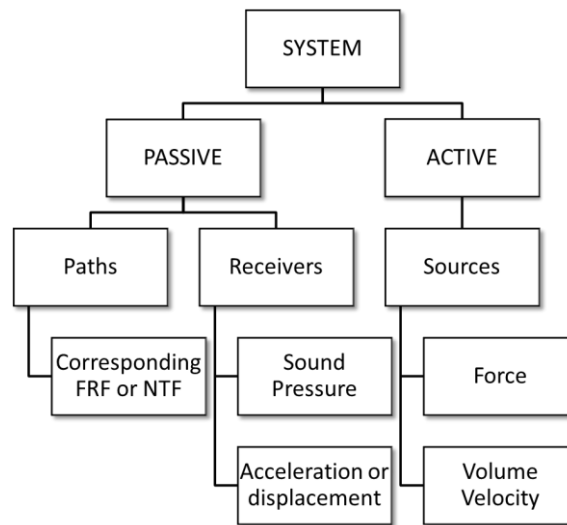
Figure 1.1 Description of a vibro-acoustic system
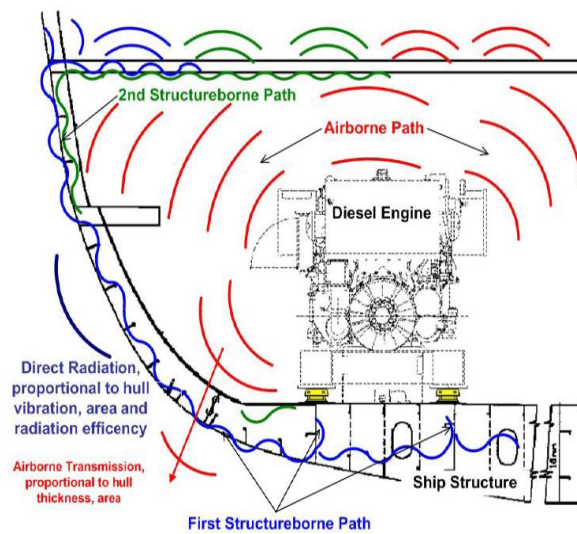
Figure 1.2 Representative transfer paths of an engine installed on a ship engine room

Traditionally, NVH characteristics of the structure had been analyzed using the Modal Analysis approach [3-7]. In this approach, vibration modes of the structure sustain motion and carry energy. Each mode is related with a characteristic frequency and vibration mode shape yielding information about the dynamic behavior of the structure. The response of a structure can be expressed as a sum of contributions from its modes. Therefore, the NVH problems can be reduced to a few dominant modes and can be solved by changing the modal frequencies. However, modal analysis approach may not be as effective when there are too many modes which contribute equally to the dynamics of the structure. In those conditions, it is not practical to trace and change all the modes in order to solve the problem. Consequently, alternative methods such as Transfer Path Analysis (TPA) have been studied to solve the NVH problems in an effective manner. TPA is a test-based or a simulation-based technique used to identify the paths dominating the vibration response at the receiver by splitting it to contributions from the internal paths [8-12]. Vibrational energy, created by an exciting force, flows through a set of known paths to a

receiver location. Once the dominant paths are determined, the problem is reduced to find a solution for minimizing or eliminating their contributions. After initial development in the early 90's, TPA has been extensively used as an effective tool in order to solve NVH problems by using experimental data, especially in the automotive industry. TPA mainly involves 3 main subtopics which are related to each other, as shown in Fig.1.3. In cases when the goal is to determine the operational forces acting on the structure, especially on the purpose of source localization or structural health monitoring, Operational Force Identification (OFI) subtopic of TPA can be used. If one is just interested in the operational response of any point, Vibration Response Prediction (VRP) subtopic of TPA can be applied after OFI. This topic can be implemented for design optimization, component selection or condition monitoring purposes. Final subtopic of TPA is called Path Contribution which actually reveals the problematic path or source. In this topic, the dominant paths and the contribution of each path to the response are determined in order to solve the NVH problem. In this dissertation, the vibration response prediction subtopic is taken into consideration, as explained in the next section.

Figure 1.3 Subtopics of transfer path analysis

1.1 Introduction to Vibration Response Prediction

For complex structures coupled with various links, predicting the vibration response at the point of interest is of great importance in terms of design optimization and component selection especially at where the response cannot be measured due to some physical constraints. If one can predict the vibration response of any point on the structure, modifications can be easily implemented such as changing the impedance of some of the components, increasing the local stiffnesses and retuning the mount rates of the machinery etc.

1.2 Motivation, Research Goals and Contribution

There are many limitations of the existing vibration prediction methodologies and some of these challenges have been explored in the literature to find a combination of fast, easy and reliable methods [13-19]. In order to contribute to the literature within the scope of vibration response prediction, the following research goals have been defined for this thesis.

- Investigating the advantages and disadvantages of the existing vibration response prediction methodologies
- Improving the existing methods in terms of measurement effort, flexibility and easiness.
- Investigating the effect of measurement errors on the prediction results.
- Investigating the effect of rubber components which may expose non-linearity to the structure.
- Presenting a new approach which is more practical and reliable compared to the existing methods for vibration response prediction.

First contribution of this dissertation is to present a unique approach for using the direct inversion method in predicting the vibration response of the coupled structures. Differently from the classical methods, a measurement approach is presented in which the measurements are performed at the source side and the cross-coupling effects are taken into consideration. Effect of the existing measurement noise and added mass on the accuracy of the prediction results are also demonstrated.

One of the major contributions of this dissertation is to present the use of Tikhonov regularization with the cross validation functions for improving the vibration prediction results. Tikhonov regularization is the process of using additional information to solve an ill-conditioned problem of the matrix inversion method. In the matrix inversion method, unconstrained least squares solution is constrained by applying Tikhonov regularization and hence, the results are improved. The most effective cross validation function for selecting the regularization parameter is presented with a case study of a rigidly-linked structure.

Another major contribution of this dissertation is to develop a hybrid methodology for predicting the vibration response of structures coupled by rigid and/or elastic couplings. In this proposed hybrid methodology, numerical modeling results are integrated with the experimental measured vibration data. The proposed methodology is validated by implementing a case study of a rubber-linked structure. This method plays an important role especially when measuring the transfer functions is not feasible due to the complexity of the structure and the measurements are affected from the existing noise.

The other major contribution is to propose a metric for selecting the measurement points at where the exciting forces are to be identified as the first step for vibration prediction methodology. These so-called force identification points must be selected properly such that representative dynamics of the structure is included in the matrix to be

inverted. This metric is composed of average condition number of the FRF matrix across the whole frequency of interest.

Another contribution is determining the effect of rubber hardness on the vibration response prediction for the rubber-linked structures.

Overall, this dissertation provides methodologies and relevant considerations for predicting the vibration responses at the structures coupled with rigid or elastic couplings and demonstrates the considerations via case studies composed of rigidly and rubber-linked structures.

1.3 Organization of the Dissertation

The dissertation work is divided into 6 chapters. Chapter 2 presents the VRP methodologies including Moore-Penrose pseudo inversion, dynamic stiffness method, direct inversion method and transmissibility matrix method. Considerations for the methods are also discussed. Chapter 3 focuses on VRP methodology based on the matrix inversion technique for rigidly-linked structures with experimental and numerical studies. Tikhonov regularization technique with the validation functions is investigated for improving the prediction results. Additionally, the effects of the measurement errors such as mass loading and existing noise on the prediction results are demonstrated. In Chapter 4, a hybrid VRP methodology in which the numerical data is integrated with the experimentally measured data is proposed and discussed for structures having rubber connections. Hyperelastic and viscoelastic behavior of the rubber is included in the simulation model to represent the system dynamics accurately. Effect of the rubber hardness is also discussed by performing a numerical case study with different shore hardness values. Finally, in Chapter 6, all the major results of the thesis are summarized and recommendations for further studies are presented.

Chapter 2.

VIBRATION RESPONSE PREDICTION METHODOLOGIES

The major step of vibration response prediction is to identify the operational internal forces acting on the transmission paths between active and passive parts of the system. The exciting forces at the transmission paths can be directly measured or indirectly calculated. Although it seems reasonable to measure the forces in a direct way by means of force transducers, it is almost impossible and entirely impractical for complex structures due to the challenges of special load cell applications without affecting the overall dynamics of the structure. In cases where the direct measurement is possible, it usually requires structural changes to attach the force transducers and it results in a change of the dynamic characteristics of the structure.

Instead of measuring the forces directly, as in the most of the existing studies, the operating forces are identified indirectly. In indirect approaches, which have been widely studied in the literature [9, 10, 20-41], the structure itself becomes the force transducer. Once the operational forces acting on each path are calculated indirectly, the vibration response at the point of interest or target, k and the contribution of each path to that point can be predicted assuming that the system is linear and time-invariant. Partial contribution of each path to the vibration response at the target can be identified by multiplying the calculated internal force acting at the path and measured FRF between the target and the source location. By adding up these partial contributions, the response at the target is

calculated, as seen in Eq.(2.1). In addition to the calculated vibration response, the dominant transfer paths are also identified.

$$\ddot{X}_k(\omega) = \sum_{i=1}^{n} \ddot{X}_{ki}(\omega) = \sum_{i=1}^{n} F_i(\omega)H_{ki}(\omega) \qquad (2.1)$$

Using Eq.(2.1), main causes of the high contributions of a dominant path can be determined such as high transfer function, high force, high point mobility etc. Then, some remedial measures or corrections can be taken by means of reducing transfer function, retuning attachment mount rates or increasing local stiffness.

2.1 Mount Stiffness Method

Verheij [20] introduced the mount stiffness method which is mainly implemented when the connections of the structure are soft such as rubber resilient mounts. In this method, resilient mounts can be defined as "force transducers" and accurate complex dynamic stiffness data of the mounts is required [42]. The system model is shown in Fig. 2.1. Each spring represents one degree of freedom (DOF) of a structural connection, the cross-coupling between the DOFs is assumed as negligible and the mount behaves like an ideal spring [43]. The difference between operational response measured at the source (active) and receiver (passive) sides is multiplied with the complex dynamic stiffness data and the result yields the dynamic operational force in that direction, as illustrated in Eq. (2.2).

$$F_i(\omega) = K_i(\omega)\frac{\ddot{X}_{ia}(\omega) - \ddot{X}_{ip}(\omega)}{-\omega^2} \qquad (2.2)$$

where $F_i(\omega)$ (i=1..n (number of paths)) denotes internal operating force acting on the paths, $K_i(\omega)$ is the complex dynamic stiffness data and $\ddot{X}_{ia}(\omega) - \ddot{X}_{ip}(\omega)$ is the relative difference

between the acceleration of the mount at the source and the receiver side of the transfer path *i*.
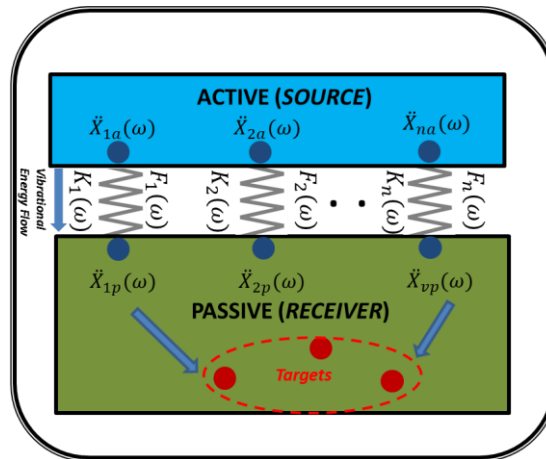
Figure 2.1 Model of mount stiffness method

Mount stiffness method seems to be the easiest, fastest and straightforward way to identify the forces. However, there are some limitations regarding the use of this method. When the transfer paths include rigid couplings or the mounts are very stiff compared to the receiver, the dynamic stiffness method cannot be implemented since the difference of the responses across the mount, as in Eq.(2.2), becomes too small. Besides, accurate dynamic stiffness data of rubber components are seldom available and dynamic measurements of these mounts are pretty expensive. Even if there is, it is only valid for a applied loading condition and amplitude since most of the mounts are nonlinear and the preload changes during operation, as reported in [43]. In this dissertation, the application of this method is not presented along with the case studies since dynamic stiffness data for the rubber mounts has not been obtained sufficiently.

2.2 Transmissibility Matrix Method

Transmissibility is basically the relationship between two vibration responses in a system measured at two locations of a structure. The use of transmissibility has been studied for several purposes such as evaluation of FRFs, finite element model updating, transfer path analysis etc. [13, 41, 44-48]

By using the operational data instead of FRFs, it is aimed to reduce the measurement time and complexity of the matrix inversion methods. In this method, the forces are replaced by the measured responses at the force identification points and the propagation paths are represented by the transmissibilities. As shown in Eq.(2.3), transmissibility can be formulated in terms of vibration responses.

$$T_{xy}(\omega) = \frac{\ddot{x}_i(\omega)}{\ddot{y}_i(\omega)} = \frac{H_{xi}(\omega)\, F_i(\omega)}{H_{yi}(\omega)\, F_i(\omega)} = \frac{H_{xi}(\omega)}{H_{yi}(\omega)} \tag{2.3}$$

where $H_{xi}(\omega)$ and $H_{yi}(\omega)$ are the corresponding transfer functions, $i = 1\ldots n$ and n stands for the number of paths.

Since the transmissibility can be defined in terms of vibration responses, the responses of the structure are grouped according to the locations whether at the active or passive side, as shown in Fig.2.2. The first step of the Transmissibility Matrix Method is to create transmissibility matrix composed of the operational measurements. The structure is excited several times by artificial forces and responses are measured for m different operating conditions, as stated in Eq.(2.4).
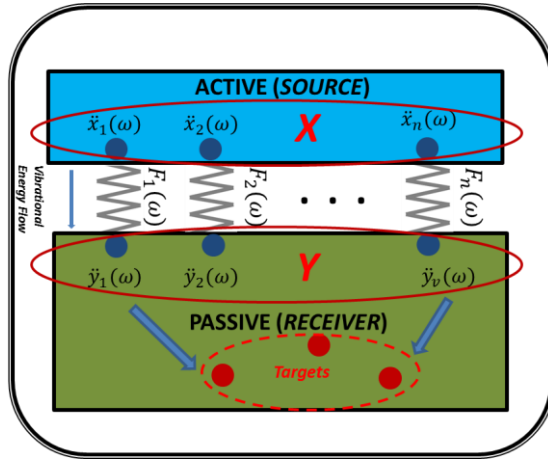
Figure 2.2 Transmissibility model

$$[\ddot{X}(\omega)] = \begin{bmatrix} \ddot{x}_1^{(1)} & \ddot{x}_1^{(2)} & \cdots & \ddot{x}_1^{(m)} \\ \vdots & \vdots & & \vdots \\ \ddot{x}_n^{(1)} & \ddot{x}_n^{(2)} & \cdots & \ddot{x}_n^{(m)} \end{bmatrix} \qquad [\ddot{Y}(\omega)] = \begin{bmatrix} \ddot{y}_1^{(1)} & \ddot{y}_1^{(2)} & \cdots & \ddot{y}_1^{(m)} \\ \vdots & \vdots & & \vdots \\ \ddot{y}_n^{(1)} & \ddot{y}_n^{(2)} & \cdots & \ddot{y}_n^{(m)} \end{bmatrix} \qquad (2.4)$$

Transmissibility matrix can be estimated from;

$$[T(\omega)] = [\ddot{Y}(\omega)] [\ddot{X}(\omega)]^+ \qquad (2.5)$$

In order to apply Eq.(2.5), the artificial excitations should be applied at the same positions for the measurements and all sources should be operating during the measurements. Besides, the number of indicators should be equal to or greater than the number of sources [49].

After determining the transmissibility matrix from the measured data of the points excited by artificial forces, the partial contribution of each path on the response of a target can be predicted by multiplying the transmissibility matrix and the in-situ measured vibration responses of the active side, as formulated in Eq.(2.6).

$$S_{yy}^{(j)}(i,i) = |T(j,i)| \, S_{xx}(j,j) \qquad (2.6)$$

where i and j represent the target and the path number, respectively. S_{xx} and S_{yy} is the autospectrum of the measured data. Therefore, the total response at the i-th receiver can be predicted as;

$$S_{yy}(i,i) = \sum_{j=1}^{n} S_{yy}^{(j)}(i,i) \qquad (2.7)$$

Since this method seems to be straightforward and practical, it strongly depends on the quality of the transmissibility matrix and the predicted responses are influenced by the position of the indicators. Therefore, some critical limitations for this method can be listed as follows [50, 51].

 a. The effect of cross coupling (Low cross-couplings between input responses are required.)

 b. The effect of coherence (Low coherence between input forces is essential.)

 c. Conditioning problems related to the identification of the transmissibility matrix

 d. The potential errors due to unconsidered paths (All active paths should be included)

 e. The position of the indicators (The indicator sensors should be placed close to the source as much as possible)

2.3 Matrix Pseudo Inversion Method

Another approach, used especially for structures having rigid connections such as bolts and bushings, is the matrix inversion method [9, 10, 20, 26, 28]. This method involves direct or reciprocal measurement of transfer functions, FRFs and vibration response measurements. In this method, before measuring FRFs between the path interface and

indicator/target points on the passive side of the structure, the source is removed and FRFs are measured between the response and source points respectively such that the corresponding path remains in place while all other path connections are disassembled from the receiving subsystem of interest. Thus, the cross-coupling effects are eliminated since the energy flows only through the remaining path during FRF measurements, FRF matrix is constituted by placing these measured FRF values to the corresponding column (path number) and row (sensor number). Passive side vibration responses at the path interface points are also measured. Operational internal force acting at each path is identified by multiplying a vector of measured vibration responses with the inverse of the FRF (accelerance) matrix, as stated in Eq.(2.8).

$$\{F(\omega)\} = [H(\omega)]^{-1}\{\ddot{X}(\omega)\} \qquad (2.8)$$

The main point in this method is that the number of response points (m) to be measured should be larger than the number of forces to be identified or so-called paths (n). Using additional information can help reducing the measurement errors, especially occurred due to the noise, which is usually present [29, 34]. As a rule of thumb, $m \geq 2n$ is usually taken [13, 29, 34, 52]. Thus, the system becomes over-determined and a least-squares solution is required. Moore-Penrose pseudo inversion technique is one of the least-squares regression analyses allowing the use of more equations than unknowns as presented in Eq.(2.9) and the system model is shown in Fig. 2.3.
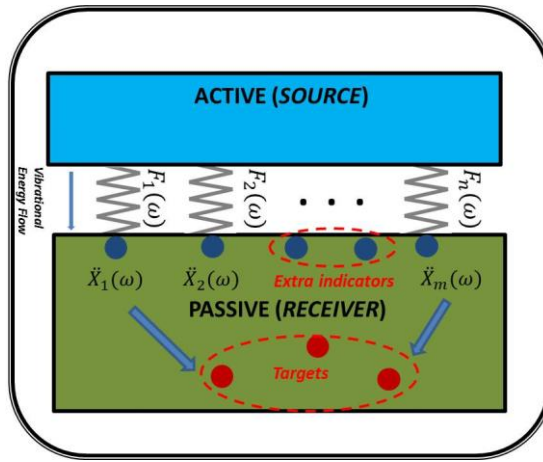
Figure 2.3 Matrix pseudo inversion model

Due to applying over-determination to reduce the measurement errors, the accelerance matrix becomes rectangular resulting in a system of linear equations which lacks a unique solution. Moore-Penrose pseudo inversion is used to compute a least squares solution to a system of linear equations, as illustrated in Eq.(2.9) [53].

$$
\begin{bmatrix} F_1(\omega) \\ \vdots \\ F_i(\omega) \\ \vdots \\ F_n(\omega) \end{bmatrix} = \begin{bmatrix} H_{11}(\omega) & \cdots & H_{1n}(\omega) \\ \vdots & \vdots & \vdots \\ H_{q1}(\omega) & \cdots & H_{qn}(\omega) \\ \vdots & \vdots & \vdots \\ H_{m1}(\omega) & \cdots & H_{mn}(\omega) \end{bmatrix}^{+} \begin{bmatrix} \ddot{X}_1(\omega) \\ \vdots \\ \ddot{X}_q(\omega) \\ \vdots \\ \ddot{X}_m(\omega) \end{bmatrix} \tag{2.9}
$$

where in $H_{mi}(\omega)$ is the frequency response function (FRF-accelerance) measured between the sensor point m and the applied force at the interface connection of transfer path, i where $i=1,\ldots,n$ (number of paths). "+" indicates the Moore-Penrose pseudo inversion and $\ddot{X}_j(\omega)$ is the operational response (acceleration) measured at sensor number, j where $j=1,..,m$ (number of sensors). Moore-Penrose pseudo inverse of accelerance matrix, H is given by:

$$
[H(\omega)]^{+} = ([H(\omega)]^{H}[H(\omega)])^{-1}[H(\omega)]^{H} \tag{2.10}
$$

where ^{H} indicates the Hermitian transpose (complex conjugate transpose). Hereby, the least-squares solution of Eq.(2.9) becomes;

$$\{F(\omega)\} = ([H(\omega)]^H[H(\omega)])^{-1}[H(\omega)]^H\{\ddot{X}(\omega)\} \qquad (2.11)$$

It should be noted that the solution should be done for each frequency, separately. The identified forces can result in errors due to the ill-conditioning of the accelerance matrix at certain frequencies and the measurement errors [30, 31, 43]. These errors are magnified by the inversion of the accelerance matrix, especially at frequencies where the condition number of the matrix is high. Condition number, which is simply the ratio of the largest singular value to the smallest one, is a good indicator for the ill-conditioning problem. High condition number indicates that the FRF matrix is ill-conditioned and the solution may not be unique.

Although over-determination improves the acceleration matrix to be inverted, the errors may still exist at frequencies where the accelerance matrix is ill-conditioned. This can be due to the fact that a few modes contribute considerably to the vibration responses near resonances. Thus, in order to improve conditioning of the matrix, the decomposition of matrix and regularization of the solution can be applied.

2.3.1 Decomposition Techniques

Matrix decomposition is a factorization of the matrix into a product of submatrices and can be used for solving a system of linear equations. Some of the decomposition techniques can be listed as follows.

- QR decomposition [54, 55]
- LU decomposition [56]
- Singular value decomposition (SVD) [26]

Among the mentioned decomposition techniques, singular value decomposition along with the Moore-Penrose pseudo inversion is applied in this dissertation.

2.3.1.1 Singular Value Decomposition

In earlier studies, singular value decomposition (SVD) algorithm has been performed for the accelerance matrix [14, 32, 57-59]. SVD is particularly effective when the coherence between the signals is quite large during the FRF measurements. In this regard, SVD method can be defined as a regularization method for reducing the effect of random errors such as noise on the measured data [26]. By applying SVD, the acceleration matrix, denoted by H^{mxn}, is partitioned in two orthogonal matrices U^{mxm} and V^{nxn} and a diagonal matrix containing singular values Σ^{mxn}, as shown in Eq.(2.12).

$$[H(\omega)] = [U(\omega)][\Sigma(\omega)][V(\omega)]^T \tag{2.12}$$

In order to improve the conditioning of the accelerance matrix, insignificant singular values should be rejected according to a threshold value. A threshold can be based on either the error in FRF measurments or in vibration responses [14, 59]. Hence, the solution is given by;

$$\{F(\omega)\} = [V(\omega)][\Sigma(\omega)]^{+}[U(\omega)]^T\{\ddot{X}(\omega)\} \tag{2.13}$$

As seen in Eq.(2.13), inverting very small singular values results in higher errors in the identified forces. Rejecting this singular values prior to inversion can help to reduce the identification errors. However, rejecting singular values can also cause the loss of valuable information.

2.3.2 Regularization Techniques

In addition to pseudo-inverse (non-regularized) and matrix decomposition methods, regularization techniques can also be applied in order to overcome the effects of ill-conditioned accelerance matrix [26]. Rejecting singular values less than some threshold value means the loss of some valuable information. Additionally, a minor change in the threshold for rejection may cause significant error in the results. This problem can be prevented by regularizing the matrix via regularization techniques. Regularization is simply the process of using additional information to solve an ill-conditioning problem. One of the various regularization techniques is *Tikhonov regularization (ridge regression)* which is mainly discussed for the use in the matrix pseudo inversion method.

2.3.2.1 Tikhonov Regularization

Tikhonov regularization is commonly used for regularizing the ill-conditioned problems named for Andrey Nikolayevich Tychonoff [60]. It is also known as ridge regression and related to the Levenberg-Marquardt algorithm for non-linear least-squares problem. Tikhonov regularization has been used for the acoustic source identification [61, 62] and also considered for the inverse force identification in structural dynamics [33, 35]. Basic idea of this method is to replace the unconstrained least-squares solution by a constrained optimization problem which would provide a valid solution. Tikhonov regularization can be named as an alternative method of regularizing a matrix by means of allowing more gradual control than singular value rejection [63]. Consider the vector of predicted vibration responses that are represented as

$$\{\ddot{X}(\omega)\} = [H(\omega)]\,\{F(\omega)\} + \{e(\omega)\} \tag{2.14}$$

where $[H(\omega)]\,\{F(\omega)\}$ is the true response and $e(\omega)$ is the error vector occurred due to the combination of measurement errors and ill-conditioning problem. In an ordinary least-

squares solution, forces are determined by minimizing these errors, i.e. $min\{e^H\,e\}$ where H indicates the Hermitian transpose. On the other hand, Tikhonov applies a regularization parameter to minimize the cost function given by

$$\{J(\omega)\} = min\{(e^H(\omega)\,e(\omega)) + \lambda(\omega)\,(F^H(\omega)F(\omega))\} \qquad (2.15)$$

where λ is the regularization parameter to be determined. This cost function introduces a bias into the solution. By changing λ, the magnification of errors are tried to be limited [33]. The minimization of the cost function results in Eq.(2.16).

$$\{F(\omega)\} = ([H(\omega)]^H[H(\omega)] + [I(\omega)]\,\lambda(\omega))^{-1}[H(\omega)]^H\,\{\ddot{X}(\omega)\} \qquad (2.16)$$

Eq.(2.16) can also be rewritten by using singular value decomposition of the accelerance matrix;

$$\{F(\omega)\} = [V(\omega)]([\Sigma(\omega)]^T[\Sigma(\omega)] + [I(\omega)]\,\lambda(\omega))^{-1}[\Sigma(\omega)]^T\,[U(\omega)]^H\{\ddot{X}(\omega)\} \qquad (2.17)$$

where $([\Sigma(\omega)]^T[\Sigma(\omega)] + [I(\omega)]\,\lambda(\omega))^{-1}[\Sigma(\omega)]^T$ is a diagonal matrix having singular elements $s_i/(s_i^2 + \lambda)$ which is different from s_i^{-1}, the elements of usual $\Sigma(\omega)$. As can be seen in Eq.(2.16), the regularization parameter modifies or weights the singular values in the inverse and allows more gradual control than singular value rejection [35]. Especially when the condition number of the accelerance matrix is high, the effect of small singular values can be disregarded by selecting an appropriate regularization parameter. Since adding a regularization parameter to the singular values results in bias at some extent, it is essential to select a proper value of λ so that it will introduce negligible bias while minimizing the errors. In order to achieve this, mathematical concepts such as ordinary cross validation (OCV), selective cross validation (SCV), and generalized cross validation (GCV) are used to choose the optimal value of λ. In this dissertation, these concepts are

applied for the rigidly coupled planar surfaces and comparison results will be presented in Chapter 3.

2.3.2.1.1 Ordinary Cross Validation (OCV)

Cross-validation is based on removing one of the data points and then solving the inverse problem using all of the remaining data points, which is called as *'leave-out-one'* [64]. In this method, out of *m* responses, *(m-1)* are used initially in the force identification. Identified forces are then used to recreate the remaining response. This predicted response is compared with the response of the removed data point and in this way, the prediction error is obtained. This process is repeated for each data point to be removed and the sum of the squares of all these predicted errors is a measure of chosen λ. Different values of λ are applied and the accuracy of the predicted response indicates the effectiveness of the chosen λ. For series of values of λ, $\Delta(\lambda)$, OCV function, is calculated for each frequency, thus frequency, ω is omitted for the sake of brevity, as shown in Eq.(2.18).

$$\Delta(\lambda) = \frac{1}{m} \sum_{k=1}^{m} \left| \ddot{X}_k - \{H_k\}\{F_k\} \right|^2 \tag{2.18}$$

where F_k is the force identified with k^{th} element of the response left and H_k is the accelerance row vector containing the transfer functions from the *n* force locations to the kth response location. Equation (2.18) can be rewritten in matrix form as,

$$\Delta(\lambda) = \frac{1}{m} \left\| B_k(\lambda)\big(I - C_k(\lambda)\big)\ddot{X}_k \right\|^2 \tag{2.19}$$

where $\|..\|$ indicates the Euclidean norm, $C_k(\lambda)$ is defined as $C_k(\lambda){=}H(H^H H + \lambda\ I)^{-1}H^H$ and $B_k(\lambda)$ is the diagonal matrix of which the entries are $1/(1 - c_{kk}(\lambda))$ and c_{kk} is the kk^{th} entries of $C_k(\lambda)$. The value of λ that corresponds to the minimum of $\Delta(\lambda)$ is defined as the optimal value of λ.

$$\lambda = argmin[\Delta(\lambda)] \tag{2.20}$$

2.3.2.1.2 Generalized Cross Validation (GCV)

In some cases, the identified force is found to be zero when $\ddot{X}_k$ is omitted from the accelerance matrix. Thus, reconstructed $\ddot{X}_k$ happens to be zero. Consequently, the matrix $C_k(\lambda)$ in Eq.(2.19) becomes diagonal. In this case, the OCV function is independent of the choice of λ so that OCV method will not function very well in near diagonal cases, as follows;

$$\Delta(\lambda) = \frac{1}{m}\sum_{k=1}^{m}\left|\ddot{X}_k\right|^2 \tag{2.21}$$

Golub et al. [65] presented GCV method which is basically a modification of the OCV method. In this method, it is stated that any estimate of λ should be invariant under rotation of the measurement coordinate system and GCV function is a weighted version of OCV function, as shown in Eq.(2.22).

$$\Delta(\lambda) = \frac{1}{m}\sum_{k=1}^{m}\left|\ddot{X}_k - \{H_k\}\{F_k\}\right|^2 w_k \tag{2.22}$$

where w_k is the weighting function as shown in Eq.(2.23) and is used for solving the diagonal problem of the measured accelerance matrix.

$$w_k = \left[\frac{1-c_{kk}}{1-\left(\frac{1}{m}\right)Trace(C(\lambda))}\right]^2 \tag{2.23}$$

Using the singular value decomposition of the accelerance matrix, GCV function can be written as;

$$\Delta(\lambda) = \frac{\left(\frac{1}{m}\right)\left\| (I - C(\lambda))\, \ddot{X} \right\|^2}{\left[\left(\frac{1}{m}\right) Trace(I - C(\lambda))\right]^2} \tag{2.24}$$

GCV rarely results in irregular choices for λ when the GCV function has a minimum near zero regularization (i.e., at λ = 0). This is important especially when strongly regularized and smoother estimates are needed.

2.3.2.1.3 Selective Cross Validation (SCV)

An alternative method, called selective cross validation, has been developed to define the proper regularization parameter by creating a variant of OCV [66]. In this method, the minimal value (over k) of the validation errors are used instead of minimizing the sum of validation errors to select the regularization parameter, as shown in Eq.(2.25) and (2.26). The minimum validation error may correspond to the minimum value of the condition numbers of the submatrices of accelerance matrix with one row omitted.

$$\Delta(\lambda) = \left| \ddot{X}_k - \{H_k\}\{F_k\} \right|^2 \tag{2.25}$$

$$\Delta(\lambda) = \left\| B(\lambda)\big(I - C(\lambda)\big)\ddot{X} \right\|_k^2 \tag{2.26}$$

Although the measurement errors are eliminated as much as possible by making the accelerance matrix over-determined, main drawback of the pseudo-inversion method is the need to perform a large number of FRF measurements after removing the source, which results in considerable time consumption. Since the system is required to be disassembled

during the FRF measurements, the boundary conditions are not the same anymore and disassembling the structures cannot be always possible [16, 17, 67]. Besides, this method can also have some random and deterministic errors in the FRFs which is discussed in the next chapter.

2.4 Direct Inversion Method Including Cross-Couplings

The vibration response of any point depends on corresponding transfer function and the force acting on that point if there is only one transmission path. However, if more than one source or path is present, the cross-coupling terms should be taken into consideration. Cross-coupling means that the response at a particular point depends not only on the force acting on that point but also on the other internal forces [13]. Cross-coupling effects are considered by means of including all FRFs between the path inputs at the active side. Accordingly, vibration response in terms of acceleration can be written in the following form;

$$\ddot{X}_1 = F_1\,H_{11} + \, F_2\,H_{21} + \cdots + \, F_n\,H_{n1} \qquad (2.27)$$

where *n* is the number of path inputs or internal forces. As can be seen in Eq.(2.27), a high response at any point does not imply that the force acting on that location is the only contributor. Thus, unconsidered cross-coupling terms lead to a false identification of operational response at the target point. Biermayer et al [68] state in their study of a passenger car that the error can be up to 10 dB if the cross-coupling terms are not adequately included.

In this approach, force identification process is applied at the active (source) side whereas in pseudo inversion method, it is based on the measurements at the passive (receiver) side. Thus, operational measurements are performed at the connection points of the paths and FRFs are measured between the path inputs in order to consider the cross-

couplings. Moreover, in contrast to the pseudo inversion method, the paths and the source are not required to be disassembled prior to FRF measurement in the direct inversion method. A schematic representation of direct inversion model is shown in Fig.2.4.
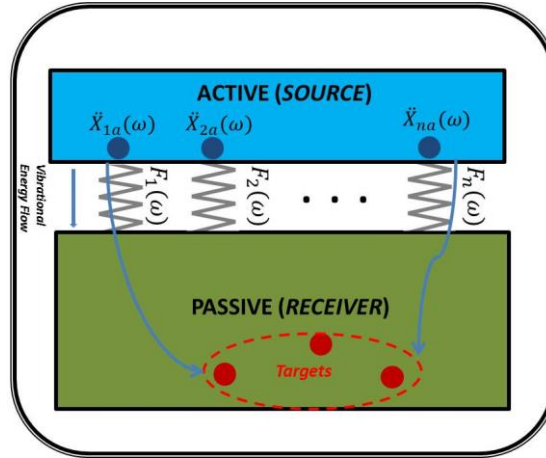
Figure 2.4 Matrix direct inversion model

A square accelerance matrix, *n x n*, is created since the number of forces and responses are equal to each other. Thus, internal forces can be identified in matrix notation by applying ordinary matrix inversion as shown in Eq.(2.28).

$$\{F_i(\omega)\} = \big[H_{ij}(\omega)\big]^{-1}\{\ddot{X}_i(\omega)\}$$
(2.28)

where *i=j* which denotes the number of paths and forces, respectively.

Presented methods in this chapter are summarized in Table 2.1 with their advantages and disadvantages. As seen in the table, for the structures having rigid or elastic couplings, the matrix direct inversion method is faster and more practical compared to other methods. Therefore, matrix direct inversion method is selected to be more suitable for the case studies presented in the next chapters.

Table 2.1 Summary of VRP methods

	Advantages	**Disadvantages**
Mount Stiffness Method	• Straightforward • Easy to apply	• Dynamic stiffness data is seldom available. • Dynamic stiffness data depends on the loading condition. • Dynamic measurements for the rubber links are pretty expensive. • Not applicable for rigid connections.
Transmissibility Method	• Straightforward • Reduced measurement time	• Prone to cross-coupling effects • Measurement points must be linearly independent
Pseudo Inversion Method	• High accuracy	• Need of large FRF measurements • Disassembling the structure is required. • Boundary conditions are not same due to disassembling. • Not practical and feasible always.
Direct Inversion Method	• Easy to apply • Reduced FRF measurements	• Reduced accuracy compared to pseudo inversion method

2.5 Considerations of Matrix Inversion Methods

Number of non-zero singular values in an accelerance matrix defines its rank. However, some of the non-zero singular values may be very small compared to other singular values. These smaller singular values amplify the error when the matrix is inverted

and also lead to the propagation of errors in the vibration responses. Thus, accelerance matrix can be defined as "almost singular" or "ill-conditioned" matrix.

The significance of the singular values can be determined by condition number which is also a function of the number of response points. The condition number is simply the ratio of the largest singular value to the smallest singular one, as stated in Eq. (2.29). High condition number implies almost singular or ill-conditioning status and is a consequence of strong modal behavior of the structure where one or a small number of modes dominate [31-33].

$$\mathrm{K}_2([H]) = \frac{\sigma_{max}}{\sigma_{min}} \tag{2.29}$$

Condition number of the accelerance matrix is a measure of the sensitivity of the pseudo-inverse. Since the accelerance matrix is inverted at each frequency, the condition number varies with the frequency. Large condition numbers exist near and at resonances and the maximum condition number of accelerance matrix of 100 is an acceptable value for the matrix inversion method. Condition number is closely related to the various factors, especially the number of participating modes, the number of forces to be identified, the damping factor at resonant, and the number of measurements.

- *The number of response measurement*: As discussed before, over-determination, in other words measuring more responses, reduces the condition number. As a rule of thumb, the number of responses included in the analysis should be at least 2 times greater than the number of forces to be identified.

- *The damping factor*: Damping is the mechanism of dissipating energy from a system by converting kinetic energy into heat. The damping factor is effective especially at resonant frequencies where the system's response is dominated by the particular mode. Thus, it becomes more of an issue. In a system with higher damping, the neighboring

modes have larger contribution to the response at that frequency. Thus, higher damping results in lower condition number, as discussed in Mas et al [29].

- *The number of forces to be identified*: Ideally, the condition number should be *1* for single force identification. Condition number of the accelerance matrix generally increases with increasing number of forces to be identified. The number of forces to be identified is limited by the number of the modes included in the analysis, which will be explained in the following section.

- *The number of significantly participating modes*: Over-determination can help reducing the condition number of the accelerance matrix especially at high frequencies, but it is usually ineffective at low frequencies where only a few modes contribute to the vibration response [31, 32, 69]. The number of participating modes (p) plays an important role in the linear dependency of the columns of the accelerance matrix [30]. In the case of low modal density, small number of modes dominates the dynamics of the structure. Thus, the operating forces would excite the same mode for the points having similar spatial locations. As a consequence, the columns or rows of the accelerance matrix become almost linearly dependent resulting in a rank deficient matrix. In this condition, the columns or rows can be defined as the linear combination of the dominant modes. Linear dependency leads to ill-conditioning of the matrix and amplifies the prediction errors when the matrix is inverted. For this reason, it is suggested that the number of forces to be identified should be less or equal to the significantly participating modes at some frequency ($n \le p$) [30, 70]. If many modes contribute to the responses, the columns of the accelerance matrix will be independent and hence, this will result in low condition number [31, 32, 69]. However, during the force identification process, it is not easy to determine the number of modes that contribute to the responses precisely, especially for complex structures. Therefore, it can be stated that this problem is generally unavoidable.

Chapter 3.

VIBRATION RESPONSE PREDICTION FOR STRUCTURES COUPLED WITH

RIGID CONNECTIONS

The aim of this chapter is to present case studies to demonstrate the vibration response prediction methodologies mentioned in Chapter 2. The vibrating structures coupled with rigid connections are of primary interest since real and complex structures have many coupled rigid links. Besides, having a low insertion loss with rigid links, the cross-coupling terms become more of an issue be considered.

In accordance with the statements, rigidly-linked set-ups are created in order to predict the vibration response at the defined target by applying the matrix inversion method. First experimental set-up consists of planar surfaces connected rigidly to each other by means of screw and nuts. The second set-up involves two substructure coupled with two rigid links.

3.1 Rigidly Coupled Planar Surfaces

In order to implement the VRP methodology and determine the effectiveness of the Tikhonov regularization technique for the rigidly linked structures, an experimental set-up is built. The set-up consists of four plates rigidly coupled to each other. The mechanical properties of the plate components are tabulated in Table 3.1. A modal shaker is fixed to Point 1, as shown in Fig.3.1 and used to generate the excitations representing the operating source. The vibration energy is transmitted through two paths resulting in two internal

forces. Since a pure one dimensional force is applied to the structure, the moments and lateral forces are introduced. However, these quantities are ignored in the calculations since it is so difficult to measure them.
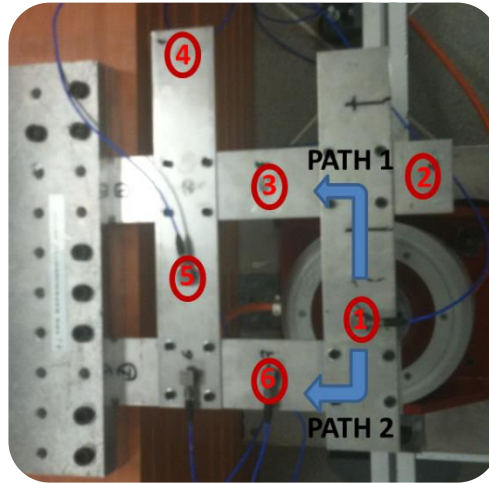
Figure 3.1 Rigidly coupled planar set-up

Table 3.1 Material and physical properties of the plate components of the set-up

Properties	Plates
Material	Steel
Young's modulus (GPa)	200
Density (kg/m^3)	8095
Length (mm)	230
Width (mm)	50
Thickness (mm)	1.5

Experimental study is composed of three parts. First, the vibration responses are measured as acceleration by using accelerometers (PZB Model 333B30). The responses are measured as complex quantities having magnitudes and phase information. Therefore, they can be derived for each frequency by using auto- and cross-spectra as

$$a_i = \sqrt{G_{ii}}\, e^{-j\angle G_{i1}} \tag{3.1}$$

where G_{ii} is the auto-spectrum of the response at point i, which gives the amplitude and G_{il} is the cross-spectrum between the reference position,1 and point i, which forms the complex part. It should be noted that Eq.(3.1) should only be used if the coherence function between a_1 and a_i is about one and the reference position should be one of the points at where the vibration response is measured [32, 71]. In this case study, frequency range of interest is selected as 0-100 Hz. Responses are measured at six points, as shown in Fig.4.1. Five of them are taken into account in order to make the system over-determined. The remaining one is selected as the point of interest, so-called target, at where the response is aimed to be predicted. Thus, measured FRFs (accelerances) and vibration response corresponding to the target are not included in the force identification algorithm. Nevertheless, the response at the target is used for comparison purposes.

Second part of the experimental study is measuring the FRFs of the structure via impact hammer (PZB model 086C03) from the source to the target locations respectively such that the corresponding path remains in place while other path connection is disassembled, as shown in Fig.3.2.(a) and (b). Thus, the cross-coupling effects are eliminated, since the energy flows through only the remaining path during FRF measurements. Accelerance matrix is constituted by importing FRFs to the corresponding columns and rows which represent the paths and the sensor numbers, respectively. In this case study, H_1, which is preferably used when there is noise in the output response signals, is taken into account as the transfer function.

(a)   (b)
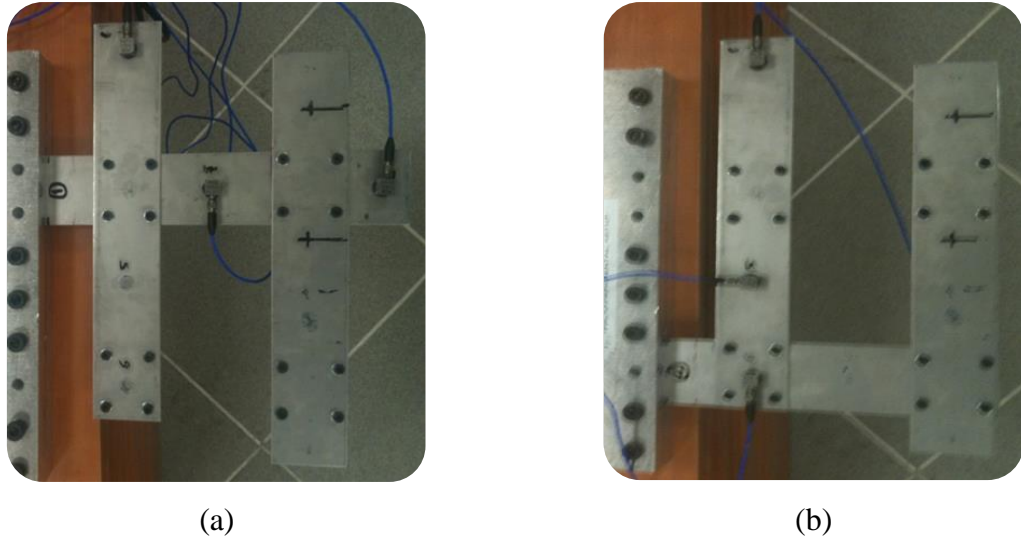
Figure 3.2 FRF measurements on the set-up;
(a) Path 1 (Path 2 is disassembled) (b) Path 2 (Path 1 is disassembled)

Finally, third part of the study is composed of data processing, implementing the presented decomposition and regularization techniques, and presenting the results as well as comparing the calculated response of the target with the measured one. This comparison serves as an indicator of the quality of the methods.

Moore-Penrose pseudo inversion method (no regularization), Tikhonov regularization with OCV, GCV and SCV concepts are applied to predict the vibration response at the selected point of interest. As presented in Chapter 2, the operating internal forces acting at each path is identified by the inversion method as follows;

$$
\begin{bmatrix} F_1(\omega) \\ \vdots \\ \vdots \\ F_n(\omega) \end{bmatrix} = \begin{bmatrix} H_{11}(\omega) & \cdots & H_{1n}(\omega) \\ \vdots & \vdots & \vdots \\ H_{q1}(\omega) & \cdots & H_{qn}(\omega) \\ \vdots & \vdots & \vdots \\ H_{m1}(\omega) & \cdots & H_{mn}(\omega) \end{bmatrix}^{+} \begin{bmatrix} \ddot{X}_1(\omega) \\ \vdots \\ \ddot{X}_q(\omega) \\ \vdots \\ \ddot{X}_m(\omega) \end{bmatrix} \tag{3.2}
$$

where $H_{mi}(\omega)$ is the FRF (accelerance) measured between the sensor point m and the internal operating force at the interface connection of transfer path, *i* where *i=1,...,n*

(number of paths, $n = 2$). "+" indicates the Moore-Penrose pseudo inversion and $\ddot{X}_j(\omega)$ is the vibration response (acceleration) measured at sensor number, j where $j=1,.., m$ (number of sensors, $m = 5$). The solution is regularized by introducing a constrained optimization via regularization parameter, as discussed in detail in Chapter 2. Hence, the force identification by Tikhonov regularization is;

$$\{F(\omega)\} = ([H(\omega)]^H [H(\omega)] + [I(\omega)] \lambda(\omega))^{-1} [H(\omega)]^H \{\ddot{X}(\omega)\} \tag{3.3}$$

where λ is the regularization parameter to be determined by the validation functions. Vibration response at the target point is predicted by implementing the following equation and compared with the measured response.

$$\ddot{X}_k(\omega) = \sum_{i=1}^{n} \ddot{X}_{ki}(\omega) = \sum_{i=1}^{n} F_i(\omega) H_{ki}(\omega) \tag{3.4}$$

The predicted response at the sensor point, S4 is presented in Fig.3.3 whereas the condition number of the accelerance matrix is shown in Fig.3.4. Moreover, prediction errors are calculated as the root mean square differences between the measured and predicted responses and tabulated in Table 3.2.

(a)   (b)

(c)   (d)
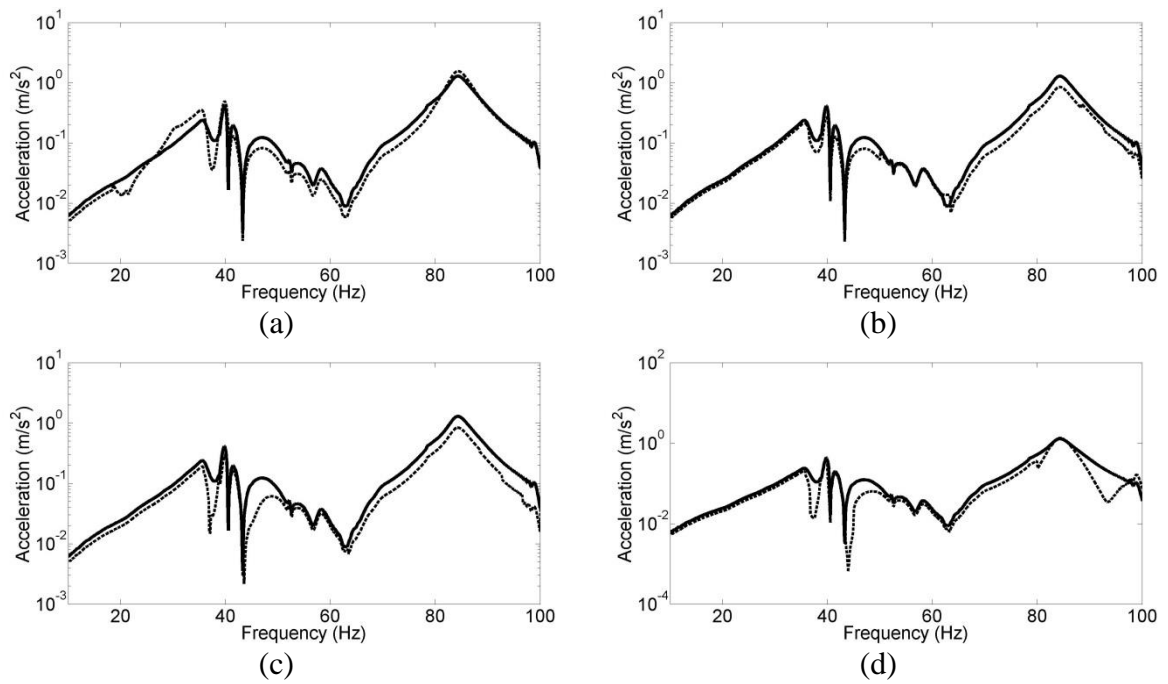
Figure 3.3 Vibration response at S4 – measured -- predicted by; (a) Pseudo inversion without regularization (b) Tikhonov-OCV (c) Tikhonov-GCV (d) Tikhonov-SCV
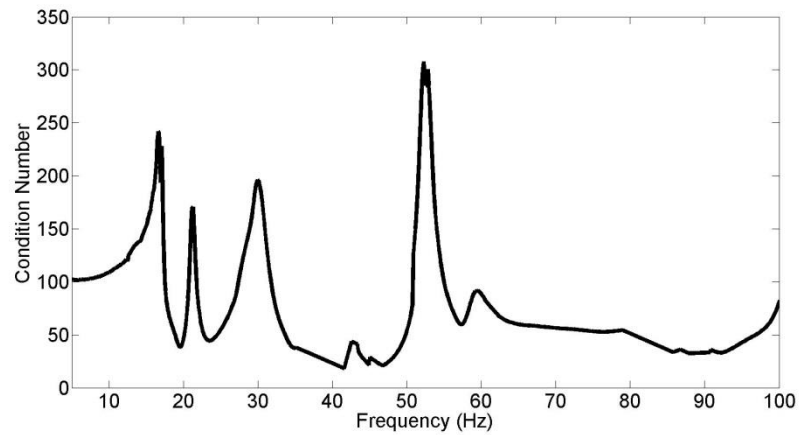
Figure 3.4 Condition number of accelerance matrix

Table 3.2 Average prediction errors in dB

Method	Average Errors in dB
Moore-Penrose Pseudo Inversion (no regularization)	3.22
Tikhonov – OCV	0.76
Tikhonov – GCV	2.82
Tikhonov – SCV	4.52

According to Fig.3.3.(a), Moore-Penrose pseudo inversion method captures the spectral character of the measured response with slight differences and it can be seen that the accuracy of the prediction increases when the condition number is low. Thus, it is validated that the condition number is a good quality indicator for VRP study, as discussed in [31, 72]. In the meantime, Tikhonov regularization based on OCV gives the most improvement on the prediction result and GCV is found to perform similarly with minor variations. However, it is observed that at specific frequencies, the prediction errors in the regularized results are higher than the errors in the non-regularized results. Considering the condition numbers at those frequencies, it is found that at low condition numbers, Tikhonov regularization degrades the result and gives rise to error amplification. In the meantime, it is observed that SCV appears as the most inefficient method for the rigidly coupled structures.

In addition to vibration response prediction, the dominating path can also be determined by generating path contribution plots (PCP). PCP shows amplitude of the partial contributions for the paths as a function of frequency. Two major peaks are observed in PCP, as shown in Fig.3.5. The dominant path for the first and second peaks (at 39 ve 83 Hz) is found to be Path 1 and Path 2, respectively.
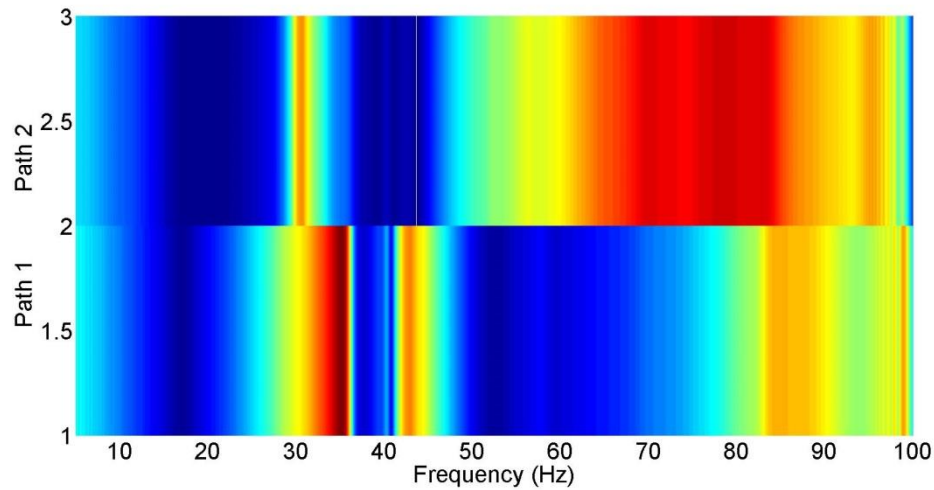
Figure 3.5 Path contribution plot for S4

3.2 Rigidly Linked Structures

In this study, vibration response prediction is discussed for rigidly–linked vibrating structures since the real and complex structures have many coupled rigid links. Differently from the previous set-up, two subsystems coupled with rigid links are used in accordance with the statements of VRP methodologies. Both pseudo and direct inversion methods are presented. Applicability and accuracy of direct inversion method, which is more practical and time efficient, is presented. Besides, the importance of the cross-coupling terms and measurement errors are discussed.

This set-up consists of two rigidly linked subsystems. The lower beam, clamped at one side, is the active part of the system while the upper beam is the passive one. The set-up is shown in Fig.3.6, the material and physical properties are tabulated in Table 3.3. The validation is conducted both experimentally and numerically.
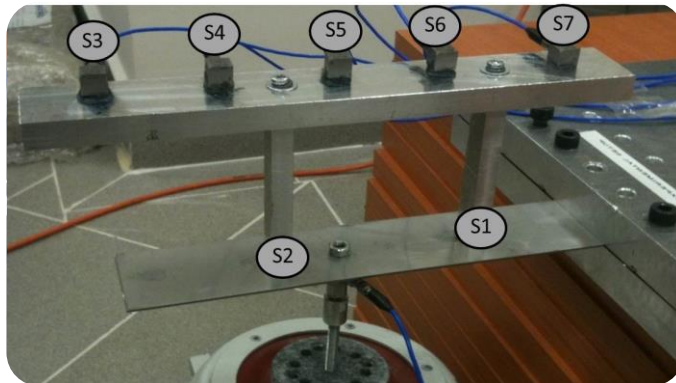
Figure 3.6 Rigidly-linked set-up

Table 3.3 Material and physical properties of the set-up

Properties	Upper Beam	Lower Beam	Links
Material	Steel	Steel	Aluminum
Young's modulus (GPa)	200	200	78
Density (kg/m^3)	8095	8095	2700
Length (mm)	265	230	86
Width (mm)	40	50	20
Thickness (mm)	15	1.5	10

3.2.1 Experimental Study

As explained in Section 3.1, in the first part of the experimental study vibrational responses as accelerations are measured by using accelerometers. A modal shaker is used as the operating source and coupled to the structure. In the second part, the accelerances are measured from the path inputs to the target locations by using the modal shaker. In this study, the frequency range of interest was selected as 0-300 Hz. As in the previous study, the moments and lateral forces are also introduced, but ignored in the calculations since they are very hard to measure. Nevertheless, the aim of this study is to estimate the internal

forces acting in the vertical direction and thus, the operational responses, assuming that the system is time-invariant and linear.

3.2.1.1 Moore-Penrose Pseudo Inversion Method Solution

First study is conducted in relation to Moore-Penrose pseudo inversion method as explained in Section 2.2. After the operational measurements are conducted, the system is disassembled at each path respectively and FRFs are measured through each path between the sensor and the source point by using the impact hammer. Accelerance matrix is constituted as by importing FRFs to the corresponding columns and rows which represent the paths and the sensor numbers, respectively. Vibration response and FRFs are measured at five sensors located at the passive side, as shown in Fig.3.6. Four of them are taken into account in order to make the system over-determined since the number of sensors should be at least equal to the number of forces to be identified, as a rule of thumb. The fifth one is selected as the point of interest, so-called target, at where the operational response is aimed to be predicted. Thus, measured transfer functions and operational response corresponding to the target are not included in the force identification algorithm. Nevertheless, the operational response at the target is used for comparison purposes.

Following the constitution of the accelerance matrix, SVD is applied to improve the condition number of the matrix and then the modified matrix is inverted by implementing Moore-Penrose pseudo inversion in order to calculate the operational internal forces, as illustrated in Eq.(3.5). After identifying the operational force, the vibration response at the selected point of interest is predicted by multiplying the correspondent FRFs with the relevant forces, as shown in Eq.(3.6).

$$\begin{bmatrix} F_1(\omega) \\ \vdots \\ \vdots \\ F_n(\omega) \end{bmatrix} = \begin{bmatrix} H_{11}(\omega) & \cdots & H_{1n}(\omega) \\ \vdots & \vdots & \vdots \\ H_{q1}(\omega) & \cdots & H_{qn}(\omega) \\ \vdots & \vdots & \vdots \\ H_{m1}(\omega) & \cdots & H_{mn}(\omega) \end{bmatrix}^{+} \begin{bmatrix} \ddot{X}_1(\omega) \\ \vdots \\ \ddot{X}_q(\omega) \\ \vdots \\ \ddot{X}_m(\omega) \end{bmatrix} \tag{3.5}$$

where $H_{mi}(\omega)$ is the FRF (accelerance) measured between the sensor point m and the internal operating force at the interface connection of transfer path, i where $i=1,...,n$ (number of paths, $n = 2$). "+" indicates the Moore-Penrose pseudo inversion and $\ddot{X}_j(\omega)$ is the vibration response (acceleration) measured at sensor number, j where $j=1,..,m$ (number of sensors, $m = 4$).

$$\ddot{X}_k(\omega) = \sum_{i=1}^{n} \ddot{X}_{ki}(\omega) = \sum_{i=1}^{n} F_i(\omega) H_{ki}(\omega) \tag{3.6}$$

where k stands for the points of interest, S3 and S4.

The predicted responses at the sensor point S3 and S4 are presented in Fig.3.7.(b) and (d) whereas the FRFs measured between sensor and the path connection points (*H31*: *FRF between sensor point 3 and path 1 connection point*) are presented in Fig.3.7.(a) and (c). The FRFs indicate that the structure does not expose similar modal contribution through the paths, which results in linear independency at the corresponding columns of the accelerance matrix, as mentioned in Section 2.2.3. Therefore, predicted responses at the targets almost match with the measured ones. However, there are still some discrepancies between the predicted and measured responses. For point S3, it is clearly observed that the variation occurs especially at 100 Hz and 150 Hz range.

(a)

(b)

(c)

(d)
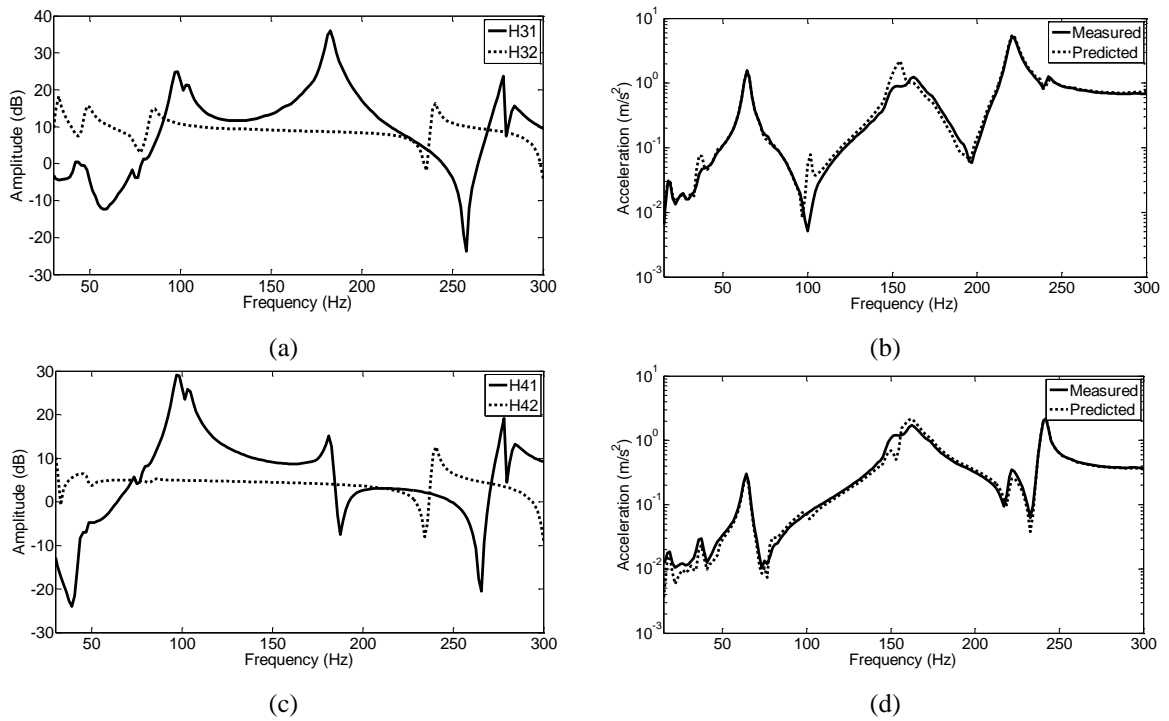
Figure 3.7 (a) FRFs measured at S3 (b) Vibration response at S3 (c) FRFs measured at S4 (d) Vibration response at S4

Figure 3.8 shows the condition number of the accelerance matrix as a function of frequency. This actually confirms that the condition number is a good quality indicator of the identification based on the matrix inversion method since one can observe noticeably large condition numbers between 100-150 Hz region. It is also clearly detected that over-determination reduces the condition number of the accelerance matrix at higher frequencies, but it is ineffective at lower frequencies where only a few modes contribute to the response, as discussed in [31-33, 73]. However, at higher frequencies, where the modal contribution is greater, over-determination gives significant reduction in condition numbers. Since measurement errors occur in any FRF measurement, these errors are amplified by the inversion of the accelerance matrix, especially at frequencies where the condition number is high and thus, the condition numbers serve as the parameters influencing the error amplification. Over-determination and singular value decomposition

improve the conditioning of the matrix and reduce the effect of the measurement errors but cannot exactly compensate for them.
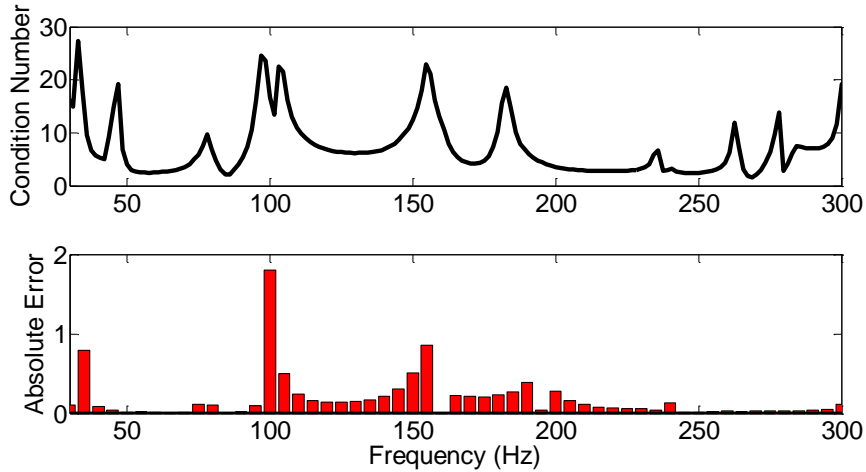
Figure 3.8 Condition number of the accelerance matrix

3.2.1.2 Direct Inversion Method Solution

Matrix direct inversion method, presented in Section 2.4, is also applied for the same experimental set-up in order to determine its effectiveness. The schematic representation of the set-up and measurements is illustrated in Fig.3.9.(a) and (b). Vibration responses are measured as acceleration at S1 and S2 located at the path inputs while the responses at the target locations are just measured for comparison purposes. In the meantime, FRFs are measured between the path inputs and the targets at the passive side without disassembling the set-up.

(a)   (b)
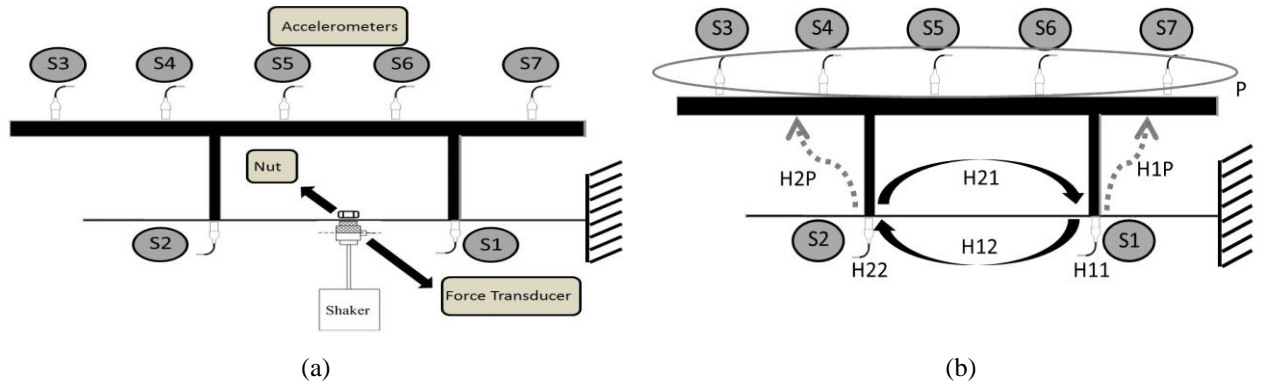
Figure 3.9 (a) Vibration response measurements (b) FRF measurements for matrix direct inversion method

FRF matrix is constituted by importing FRFs measured between the path connection points in order to include the cross couplings, as illustrated in Fig.3.9.(b). Exciting internal forces are identified by applying direct inversion method as in Eq.(3.7) and the vibration responses are predicted. Same points, S3 and S4 are selected as the targets on the purpose of comparison with Moore-Penrose pseudo inversion method and predicted results are compared with the measured ones in Fig.3.10.

$$\begin{Bmatrix} F_1(\omega) \\ F_2(\omega) \end{Bmatrix} = \begin{bmatrix} H_{11}(\omega) & H_{12}(\omega) \\ H_{21}(\omega) & H_{22}(\omega) \end{bmatrix}^{-1} \begin{Bmatrix} \ddot{X}_1(\omega) \\ \ddot{X}_2(\omega) \end{Bmatrix} \qquad (3.7)$$

As shown in Fig.3.10, the direct inversion method captures the spectral character of the measured response with slight magnitude differences and it can be stated that there is an acceptable correlation between the measured and predicted results.

(a)   (b)
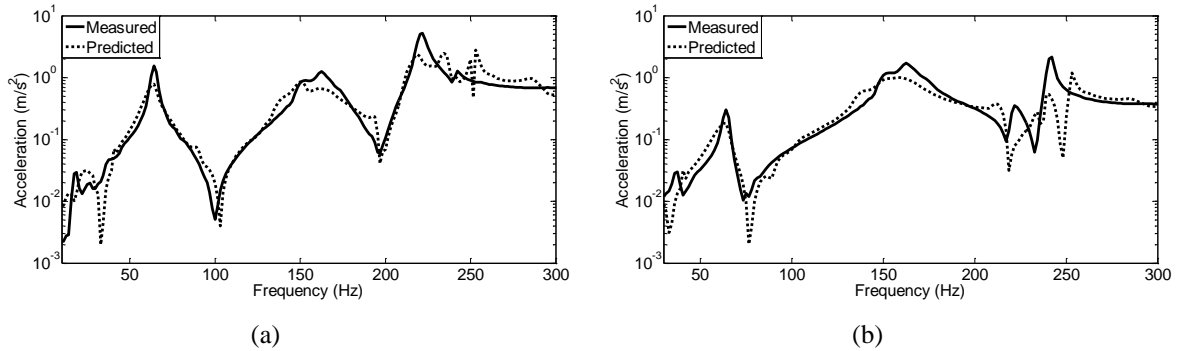
Figure 3.10 Vibration responses; (a) at S3 (b) at S4

In addition to the VRP study, the question is now to determine the path dominating the response at a particular frequency by these methods. For that purpose, path contribution plots (PCP) are generated. PCP shows the amplitude of the partial contributions for the paths as a function of frequency. Since at 220 and 240 Hz, the response of point S3 has the highest value over the entire frequency range, the PCPs are exhibited between 200 and 300 Hz in Fig.3.11.

(a)   (b)
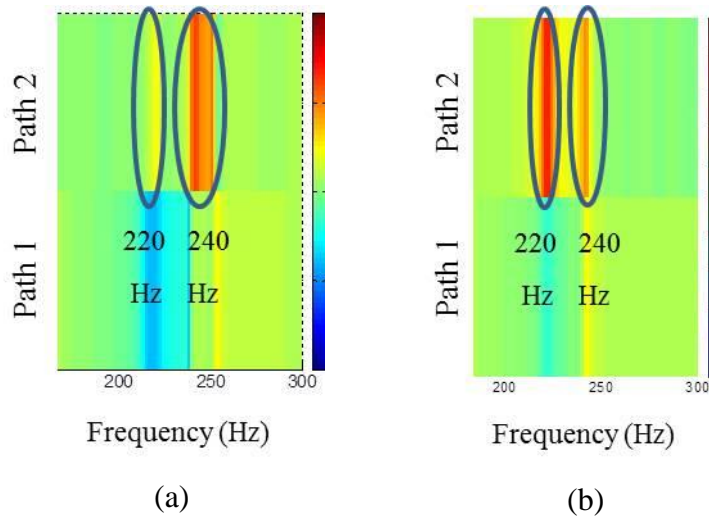
Figure 3.11 Path Contribution Plots (PCP) for S3; (a) Direct Inversion Method (b) Pseudo Inversion Method

As shown in Fig.3.11, path 2 is determined as the dominant path on the response at 220 and 240 Hz. and both methods have a good agreement on the path contribution with corresponding frequencies.

According to the predicted responses by the direct inversion method, there are some unavoidable discrepancies which can be occurred due to the combination of some assumptions and measurement errors. In this study, the rotations, moments and lateral forces are neglected as in many experimental analyses [52]. Additionally, it is assumed that the sum of energy flowing through all paths to the target is always equal to the total energy as measured at the target location. However, there may be transmission loss through the active subsystem.

In addition to the linear energy flow assumption, there are also measurement errors in the experimental studies. The testing process is prone to errors introduced by various factors. Among these, one of the factors is the mass loading effect of the force transducer. As illustrated in Fig.3.9, a modal shaker is used for the FRF measurements and connected to the structure through a force transducer by means of a screw and nut. Since this transducer is mounted on the structure, the dynamic of the set-up is changed and thus, the measured FRF contain errors consequently, as discussed in [74-76]. Besides, excessive tightening of the nut can result in additional inertia mass. This mass loading effect can be significant since the set-up is a light-weighted structure. Another factor is the alignment of the shaker. Misalignment is an important item of concern which can cause distortion of the measured data [77]. Moreover, measured data is usually contaminated with other adverse effects such as noise.

3.2.2 Numerical Study

A numerical case study is also presented to verify the method as well as to demonstrate the effects of the mass loading and noise on the experimental results of the VRP

methodology. A Finite Element Model (FEM) of the experimental set-up is built to perform the numerical study, as seen in Fig. 3.12 and the flow chart of the numerical VRP study is illustrated in Fig. 3.13.

The structure is excited at the lower beam by using the force spectral data obtained from the experimental study. The energy created by the excitation force propagates through the links to the upper beam. Thus, internal forces are introduced at the links and identified by applying both methods mentioned in Chapter 2. However, numerical study conducted in accordance with direct inversion method is presented for the sake of brevity. Accelerance matrix, a size of *2x2*, is composed of transfer functions measured at the points S1, S2 and also between each other on the purpose of including the cross-coupling effects. Vibration responses at S1 and S2 are used in identifying the internal forces with the accelerance matrix whereas the others are employed for comparison purposes. Thus, responses at the points of interest on the upper beam are predicted and compared with the actual one.
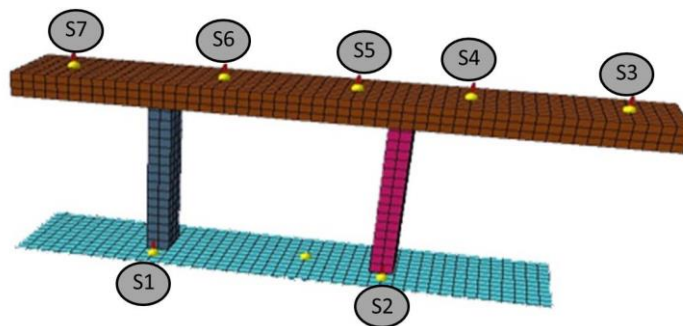
Figure 3.12 Numerical FE model of the set-up
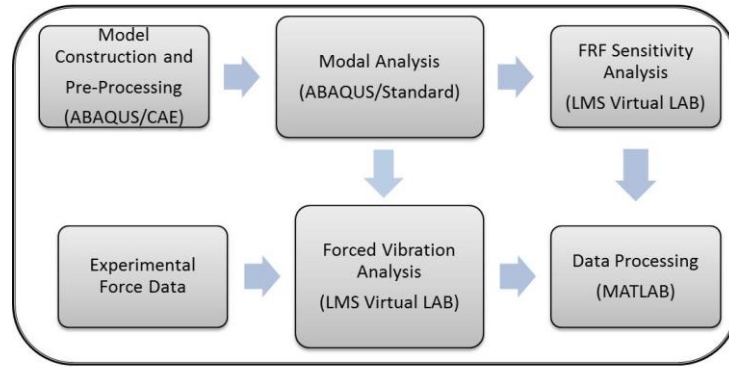
Figure 3.13 Numerical VRP study flow chart

The predicted and actual numerical response of S3 is shown in Fig.3.14. As shown in the figure, predicted response fits well with the actual one. The resonance frequencies are exactly the same while the amplitudes differ slightly. The internal operational forces are also determined without including cross-coupling terms. In other words, each internal force acting on the link is identified by using corresponding path input and its point transfer function, as follows;

$$F_1(\omega) = H_{11}(\omega)^{-1}\, \ddot{X}_1(\omega); \quad F_2(\omega) = H_{22}(\omega)^{-1}\, \ddot{X}_2(\omega) \tag{3.8}$$

From Fig.3.14, it can be clearly observed that the prediction without including cross-coupling terms increases the overall error with about a rate of 10-12 % in the frequency band. Note that, a similar behavior is observed for the other measurement locations (eg. S4, S5, S6 and S7).
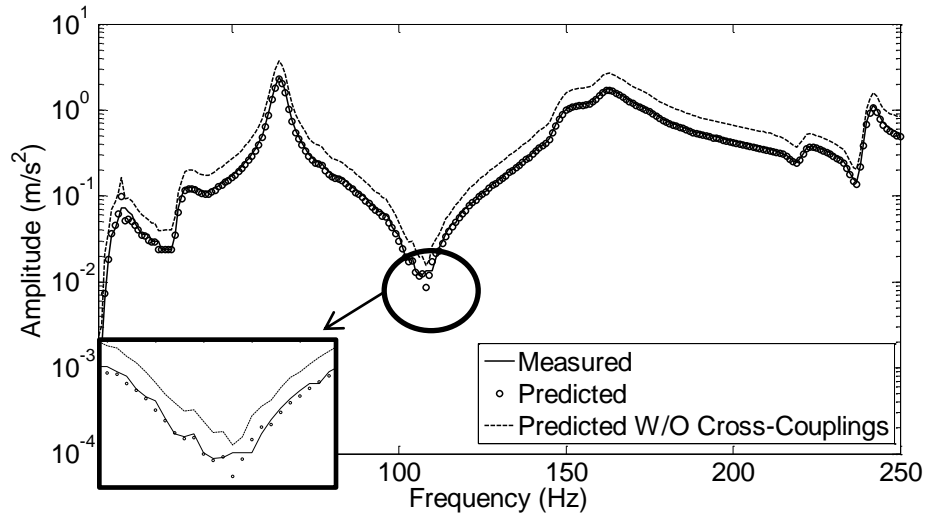
Figure 3.14 Predicted vibration response at S3

The comparison of measured and predicted responses can be accomplished by using a metric developed in previous validation studies [78, 79]. This metric is based on the variance of the calculated and measured values. Variance, σ^2, is a measure of variability involving the deviations from the mean and gives the extent of concentration around the mean value [80]. The change of the variance with frequency can be defined by the power spectral density (PSD), S_{xx} which gives the power of the signal as a function of frequency.

$$\frac{\partial \sigma^2(\omega)}{\partial \omega} = S_{xx}(\omega) \tag{3.9}$$

Hence, the variance can be expressed as a function of frequency range;

$$\sigma^2(f_1, f_2) = \int_{f_1}^{f_2} S_{xx}(\omega) d\omega \tag{3.10}$$

The variance, shown in Eq.(3.10) can also be described as the cumulative absolute variance which is the contribution of frequency components within a frequency range to

the total variance [81]. The accuracy of the methods is determined by utilizing the square root of the variance, σ. For both experimental and numerical studies, the ratio of σ between the measured and calculated responses with applied methods is tabulated within a number of bandwidths in Table 3.4. The value of such metric highlights the correlation level between the measured and calculated results. The unity (1) value indicates a perfect match and values closer to unity are accepted as satisfactory.

Table 3.4 Comparison of measured and calculated responses

Applied Methods		$\sigma_{calculated}/\sigma_{measured}$				
		0-50 Hz	50-100 Hz	100-200 Hz	200-300 Hz	0-300 Hz
Pseudo Inversion	Experimental	1	0.80	1.03	0.85	**0.91**
	Numerical	1	1	1.13	1.19	**0.99**
Direct Inversion	Experimental	1.12	1.63	0.37	0.70	**1.37**
	Numerical	0.99	0.90	0.87	1.15	**1.07**

According to Table 3.4, the pseudo inversion method reveals a bit more accurate result than the direct inversion method does over the entire 0-300 Hz range. This is due to the fact that since the active side is separated from the passive side while determining the transfer functions, the cross-coupling effects are prevented.

As shown in the results, in the numerical study the predicted response matches with the actual one considerably well compared to the experimental study. The difference between the numerical and experimental results is assumed to be occurred due to the measurement errors. These errors are magnified by the inversion of the accelerance matrix. Since real measurements are never made under perfect conditions, further simulations are focused on the measurement errors and applied to identify the significance of these effects on the VRP study. These adverse effects are composed of mass loadings due to the force transducer and shaker connections and the existing noise during the FRF measurements.

3.2.3   Demonstration of Mass Loading Effects on the VRP

The mass loading effects occurred due to the force transducer and the shaker connections are usually ignored in the experimental studies, based on the assumption that they are negligible compared to that of the structure. Nevertheless, if the structure is light-weighted, then these mass effects can be significant. Thus, in order to demonstrate the effect of the mass loading on the operational response predictions, point mass is intentionally added to the shaker connection points at the path inputs during the numerical FRF analysis. After obtaining the FRF data altered by the additional mass loadings at the path inputs, the accelerance matrix is constituted and the direct inversion method is applied. As can be seen in Fig.3.15, the condition number of the accelerance matrix is increased at each frequency and thus, the error in response prediction is expected to be larger compared to the ideal numerical result. The vibration response of S3 is presented in Fig.3.16. It is observed that the discrepancies are occurred especially between 200 and 250 Hz, as expected according to the condition number. As illustrated in Fig.3.16, mass loadings can affect the results having discrepancies between 20 and 30 dB in magnitude and similar results in the experimental study are also observed at mentioned frequency range in Fig.3.10.(a).
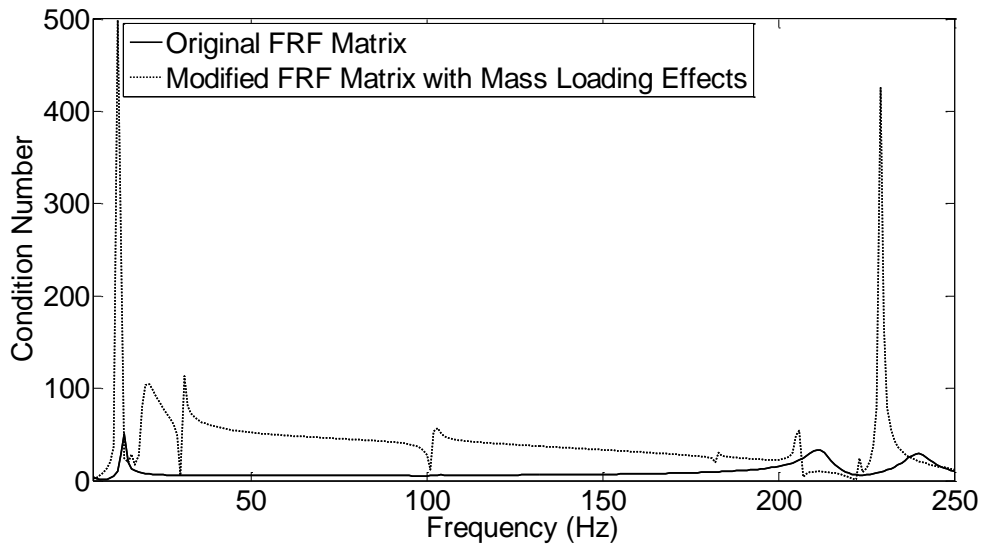
Figure 3.15 Condition number of the accelerance matrix
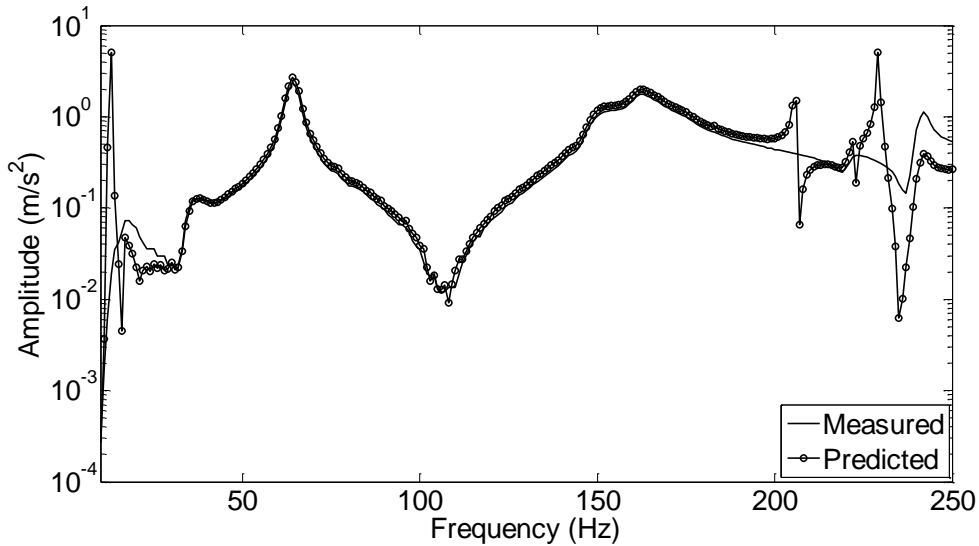
Figure 3.16 Vibration response at sensor point S3

3.2.4   Demonstration of Noise Effects on the VRP

Along with the mass loading effects, FRFs measured in reality are also contaminated with other adverse effects such as noise. In any FRF measurements, noise exists at both the input and the output channel. For frequencies close to resonance and anti-resonances, the

noise can be ignored since the vibration response is dominant. However, for the other frequencies the noise can affect the FRF measurement from both ends [82]. In this study, further simulations are conducted to examine the result of the operational response prediction in the case of noisy FRF data and consequently accelerance matrix. Thus, FRFs are numerically contaminated with additive white noise with a degree of contamination being 5 % which result in ill-conditioned accelerance matrix, as illustrated in Fig.3.17. The procedures of the direct inversion method are applied again and the operational response of sensor S3 is predicted. The contamination of the FRF data with a degree of 5 % results in errors up to 6 dB as shown in Fig.3.18.
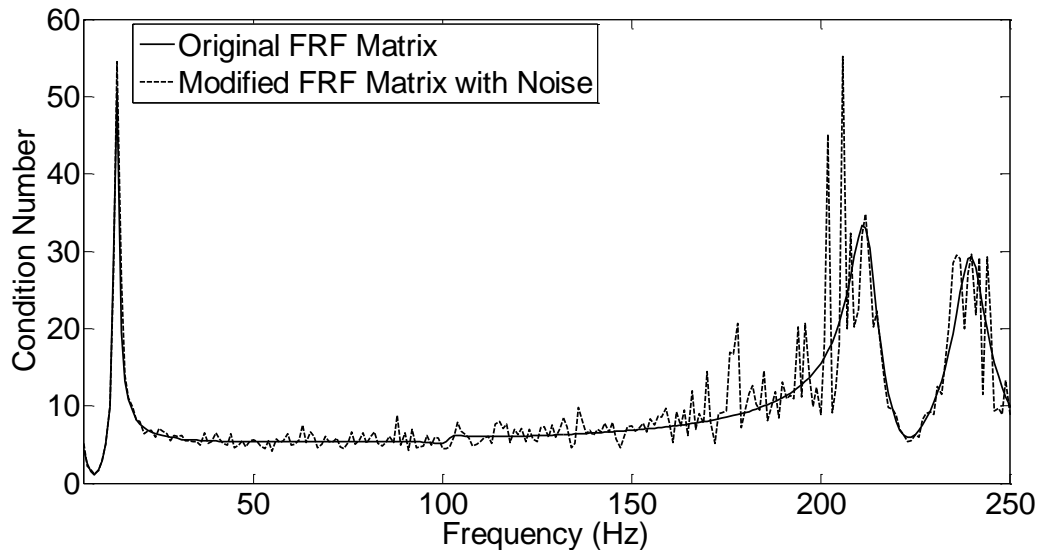
Figure 3.17 Condition number of the accelerance matrix
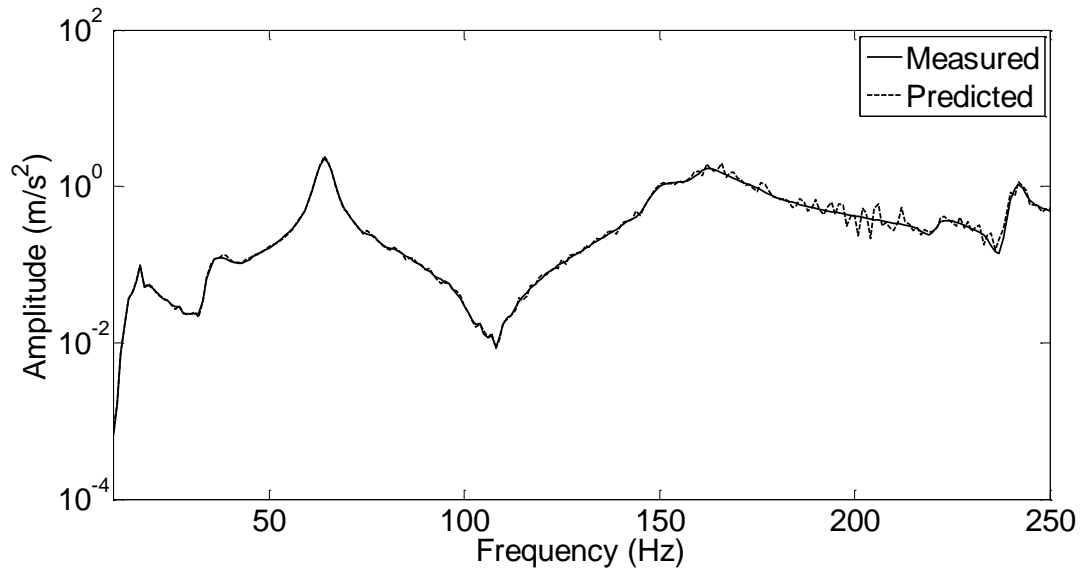
Figure 3.18 Vibration response at sensor point S3

As can be observed in the numerical results, the experimental FRF measurements are prone to the errors due to mass loadings and existing noise. These errors are almost unavoidable and result in larger condition numbers in accelerance matrix. Since the matrix is inverted, these errors are magnified at particular frequencies, as presented in [57, 58] and thus, some discrepancies are determined at the operational response identified by the direct inversion method, as also seen in the experimental results. It can also be concluded that if the primary concern is the VRP study and path contribution in terms of design optimization, condition monitoring, taking remedial measures, the direct inversion method can be implemented for this kind of structures since these methods require less effort and measurement time.

3.3 Summary and Conclusions:

In this chapter, the vibration response prediction based on the matrix inversion methods for the structures with rigid connections is discussed with the numerical and experimental case studies. In the first case study, a rigidly coupled planar structure is taken into account. Moore-Penrose pseudo-inversion method and Tikhonov regularization along with the parameter selection concepts on the VRP are applied. Over-determination as well as singular value decomposition is also considered to improve the accelerance matrix to be inverted in order to identify the operational internal forces and then, predict the vibration response at the point of interest. It is shown that Moore-Penrose pseudo inversion method gives satisfactory prediction results with some discrepancies at specific frequencies where the condition number is high. Thus, it can be stated that the condition numbers serve as the parameters influencing the prediction errors. Tikhonov regularization technique with OCV and GCV is found to be robust in improving the prediction results in the case of rigidly coupled structures. On the other hand, SCV method cannot be defined as an effective concept. Considering all Tikhonov regularization results, it is seen that it does not improve the prediction results considerably when the condition number is low. Thus, it may not be beneficial to apply regularization at all frequencies and the condition number should be taken into consideration. As a consequence, pseudo-inversion technique is proven to be reliable but its application requires huge effort as well as extensive time since the paths should be disassembled and a huge amount of FRF measurements are needed.

On the purpose of seeking faster and easier methods, the direct inversion method is investigated in the second case study which is composed of a rigidly linked structure. Compared to pseudo-inversion technique, this method is less time consuming, less challenging and the real boundary conditions are present since no disassembling is required. However, it has some limitations besides its advantages. All structures exhibit a certain amount of cross-coupling between the path inputs. Therefore, reliability of the

predicted responses strongly depends on the degree of cross-coupling since the system is not required to be disassembled. Accordingly, the vibration response of the target is predicted by implementing this method which includes the cross-couplings between the path inputs and a comparison metric based on the variance is used for determining the effectiveness with respect to defined frequency bandwidths. The results show that including cross-coupling terms improves the results with a rate of about 10-12 % and the predicted responses agree quite closely both in character and magnitude having some discrepancies occurred due to the measurement errors. As demonstrated in the numerical study, the operation responses identified by the direct inversion method are prone to measurement errors such as mass loadings and existing noise. These errors are almost unavoidable and result in discrepancies at particular frequencies of the predicted response, as demonstrated in the case study. As a consequence, the direct inversion method including cross-couplings can be implemented for the rigidly linked structures if they are almost impossible to be disassembled and the primary concern is predicting the operational response as well as determining the dominant paths in terms of structural health monitoring and design optimization.

Chapter 4.

VIBRATION RESPONSE PREDICTION FOR STRUCTURES COUPLED WITH ELASTIC CONNECTIONS

As mentioned in previous chapters, a dynamic system yields a vibrational energy flowing through the transfer paths. The most common way to reduce the energy flow to the receiver is to either reflect the vibrational energy by altering the impedance or to dissipate it by generating additional damping [83]. The former is achieved by using a much elastic and softer link compared to the receiving structure. These softer components are called as the vibration isolators or mounts. Rubber mounts have been used in the field of automotive vehicle engine mounting systems to isolate the vehicle chassis from the engine vibration [84]. In an engine mount, the elastic properties, namely dynamic stiffness, of rubber store and return most of the energy to the engine at higher frequencies resulting in transmission reduction to the vehicle chassis. On the other hand, the viscous properties, namely damping, are effective in terms of reducing the low frequency vibration generated during idling of the engine [85-88]. Therefore, the dynamic properties of rubbers make it an excellent choice for vibration isolators or so called transfer paths. Among these characteristics, they are compact, easily available, cost effective and maintenance free.

The main goal of this chapter is to propose a hybrid VRP methodology in which the numerical data is integrated with the experimentally measured ones. Then, the proposed

methodology is applied for a rubber linked structure to predict the vibration response with the considerations.

4.1 Hybrid Vibration Response Methodology

As discussed Chapter 2, major step of the vibration response prediction (VRP) is to identify the exciting forces acting on the structure. However, this may not be possible due to the complexity of the structure and the challenges of load cell applications. Consequently, indirect methods have been widely studied in the literature [9, 10, 20-35]. One of the indirect methods, matrix inversion method basically involves multiplication of a vector of vibration responses with an inverted matrix constituted by the frequency response functions (FRFs). The main drawback of this method is the need of the FRF measurements. However, measuring FRFs are sometimes not possible especially for complex structures. Even when it is possible; it is very time consuming and prone to significant errors based on excitation, environment, sensor, structure and unconsidered sources. The possible sources of the above measurement errors are shown in Fig.4.1. [74, 75, 89-93].
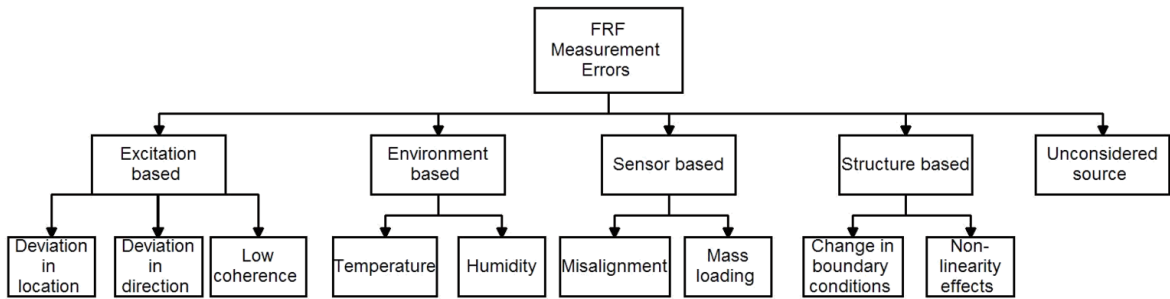
Figure 4.1 Possible errors in FRF measurements

Modal behavior of the structure has also an influence on the reliability of the matrix inversion method. In the condition that the structure has a strong modal behavior where one or few modes dominate the responses at given frequencies, the rows or columns of the FRF matrix become linearly dependent. Hence, the condition numbers of the FRF matrix are

quite high at these frequencies and in this case, the solution may not be unique and the FRF matrix can be defined as "almost singular" or "ill-conditioned" [30, 31].

As discussed in Chapter 2, combination of the insufficient modal contribution and measurement errors cause erroneous results in the force identification process and so, in the response prediction. Thus, eliminating these problems is of great importance in order to improve the accuracy of the prediction results. Previous studies focused on either reducing the experimental measurement efforts and/or improving the conditioning of the FRF matrix. In order to overcome the experimental challenges as well as measurement errors, numerical simulations have been widely used. However, the responses required for the inverse method cannot be computed accurately in a numerical simulation.

Conditioning methods result in additional measurements and using numerical model causes reduced accuracy due to the mismatch between the simulation model and the real system. Considering these challenges, a hybrid VRP methodology, in which numerical modeling results are integrated with the experimental data, is proposed in this chapter. In the proposed hybrid methodology, the experimental errors and difficulties of FRF measurements as well as time consumption are eliminated since FRFs are calculated numerically. Moreover, inverse problem is improved by reducing the condition number of the FRF matrix. An accurate numerical model and selection of the force identification points are critical before constructing the FRF matrix. If the representative dynamics of the structure is not included in the measured FRFs due to a wrong selection of the measurement locations, the forces are not identified correctly, and it affects the accuracy of the response prediction process. Accordingly, force identification points are selected based on the "combined condition number" metric within the scope of hybrid VRP.

Hybrid VRP methodology differs from the classical VRP methods in the construction of the FRF matrix. The FRFs are obtained from the numerical model of the structure and

accelerance (FRF) matrix, $\left[H_{ij}(\omega)\right]$ of Eq.(4.1) is formed by the numerical FRFs whereas acceleration vector, $\left\{\ddot{X}_i(\omega)\right\}$ is measured through the experimental studies.

$$\{F_i(\omega)\} = \left[H_{ij}(\omega)\right]^{-1}\{\ddot{X}_i(\omega)\} \tag{4.1}$$

where $i=j$ which denotes the paths and forces, respectively. Once the exciting internal forces acting at each path are determined, the vibration responses are predicted as follows;

$$\ddot{X}_k(\omega) = \sum_{i=1}^{n}\ddot{X}_{ki}(\omega) = \sum_{i=1}^{n}F_i(\omega)H_{ki}(\omega) \tag{4.2}$$

where n is the number of paths and k stands for the target.

For obtaining accurate predictions from the hybrid VRP, an accurate numerical model of the structure must be created and validated. In this approach, two important steps must be completed before performing a hybrid VRP;

(a) Numerical FRFs on the structure must be validated using measured FRFs.

(b) Force identification points must be selected properly such that representative dynamics of the structure is included in the measured FRFs. Condition number of the FRF matrix is used as a metric to select the measurement points and it is related to the spatial position of the measurement points depending on the modal behavior of the structure.

A flow diagram of the hybrid VRP is shown in Fig.4.2. The detailed process is as follows;

(a) Create a FE model of the structure including all components.

(b) Determine the validation points at where the numerical and experimental FRFs are compared. If there are discrepancies between the FRFs over the frequency of interest, the FE model should be updated.

(c) After validation process, select m candidate points to determine best force identification points.

(d) Create combination with each set of two candidate points.

(e) Calculate coupled FRFs between the points for each combination

(f) Construct FRF matrix, $[H_{ij}(\omega)]$, *(2x2)* for each set of two measurement points *(i,j)*.

(g) Calculate the combined condition number, C_{ij} as follows.

$$C_{ij} = \frac{1}{n} \left(\sum_{\omega} K_2\big([H_{ij}(\omega)]\big) \right) \tag{4.3}$$

where *n* is the number of discrete frequencies and K_2 stands for the 2-norm condition number.

(h) Select the combination having the minimum combined condition number.

(i) Measure vibration responses at the selected points.

(j) Calculate FRFs between the selected and target points from the numerical model.

(k) Perform hybrid VRP based on the direct matrix inversion method with the set of experimental measurements and numerical FRFs.
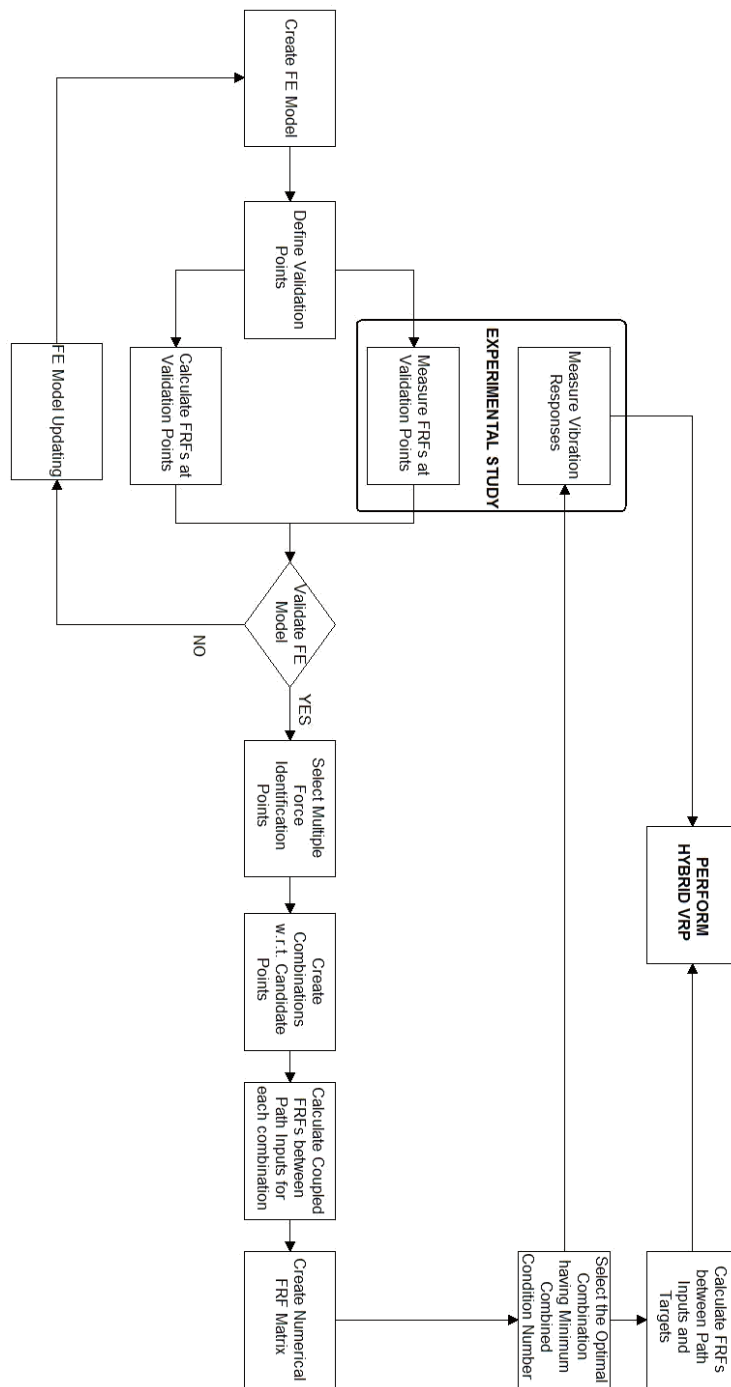
Figure 4.2 Hybrid VRP flow chart

4.2 Rubber Linked Structure

In accordance with the statements of hybrid VRP methodology and rubber theory presented in Appendix A, a rubber linked set-up is created in order to predict the vibration response at the defined target by applying the direct inversion method. This set-up, shown in Fig.4.3, consists of two subsystems coupled with two rubber mounts with a shore hardness of 75 A, product of Tekno Kaucuk A.S. The lower beam, clamped at both sides, is the passive part of the system while the upper beam is the active one.

Figure 4.3 Rubber linked set-up

The schematic representation of the experimental set-up with the force and response measurement locations, T1, T2 and T3 are shown in Fig.4.4. Equation (4.1) is used to predict the response at T1, T2 and T3. A modal shaker is fixed to the structure and used to generate the excitations representing the operating source, **F**. Although there is one operational force acting on the structure, vibrational energy flows through the rubber links resulting in internal forces. The moments and rotations are ignored in the calculations since it is very difficult to measure those quantities. Internal forces acting at each path are identified via direct inversion method and the responses at the targets are predicted as mentioned above.
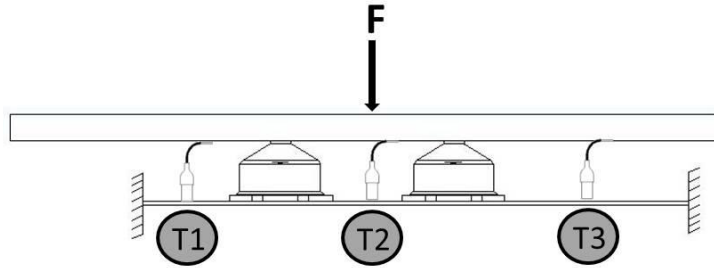
Figure 4.4 Schematic representation of the set-up

4.2.1   Numerical Model Construction and Validation

Within the scope of hybrid VRP methodology, a numerical FEM model of the set-up is created in ANSYS and shown in Fig.4.5. In order to represent the system behavior accurately in the numerical simulation, the hyperelastic and viscoelastic properties of the rubber components are obtained by experimental measurements which are presented in Appendix A.
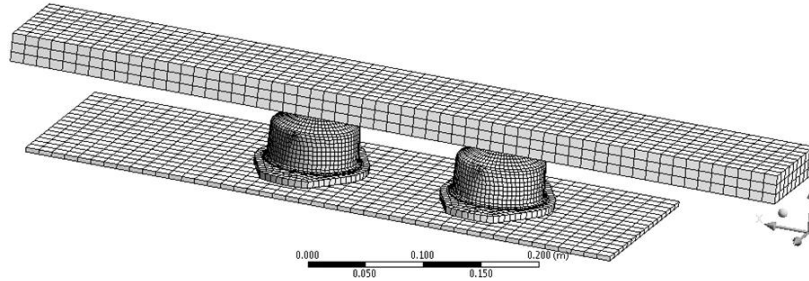
Figure 4.5 Numerical FE model of the set-up

A system with rubber components can display nonlinearity due to the hyperelastic properties of the rubber. Equation of motion of a general nonlinear system, subjected to a time dependent excitation, is as stated in Eq.(4.3).

$$[M]\{x(t)\} + [C]\{\dot{x}(t)\} + i[D]\{x(t)\} + [K]\{x(t)\} + \{G(\dot{x}(t), x(t)\} = \{f(t)\} \quad (4.3)$$

where *M, C, D* and *K* are mass, viscous damping, hysteretic damping and stiffness matrices, respectively. Nonlinearity of the system is represented by the nonlinear vector, *G* which is a function of all displacements and velocities in general case. Owing to nonlinear material properties of the model, linear harmonic analysis cannot be performed by FEM solvers. Instead, transient analysis can be considered since it results in more accurate solutions but more time consumption and computational power. The responses obtained in time domain are transformed to the frequency domain via using the numerical simulation algorithm in MATLAB, as described in Fig.4.6. In this algorithm, calculated data is divided into smaller blocks in order to compute FFTs instead of computing a single FFT for the whole data set. Overlapping, which is a process of using a percentage of the previous data block to calculate the FFT of the current data block, is applied on the measured data. When combined with windowing, overlapping increases the use of data set. Windowing reduces the effect of leakage which occurs due to the FFT calculations for aperiodic data blocks. Additionally, averages are taken to obtain a good representation of the spectrum and improve the accuracy of FFT.
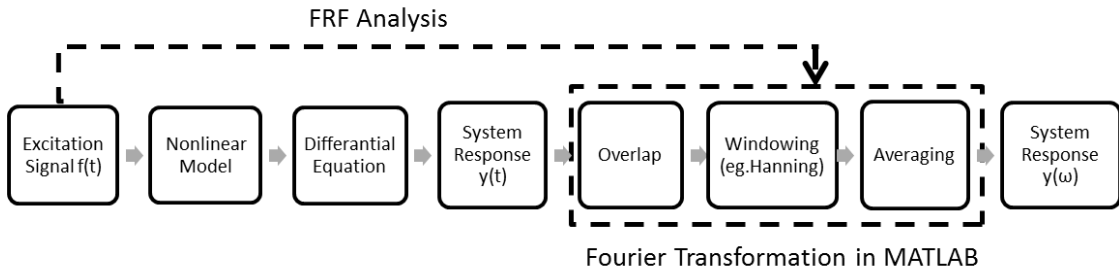
Figure 4.6 Numerical simulation algorithm

In this case study, a sine sweep signal (see Fig.4.7) is generated as the excitation signal for FRF calculation. The amplitude of the signal is taken as 1 N and sweep frequency is considered up to 100 Hz having a sampling frequency of 600 Hz. Step size is taken as 4800 and two sweeps are generated. Numerical model is excited by this sine-sweep signal and

transient analysis is conducted. Vibration responses are calculated in time domain and transformed to frequency domain by a code written in MATLAB. By applying this code, consecutive blocks of time signal are overlapped by 50 % and Hanning window is applied. Then, data in time domain is transformed to frequency domain by using the simulation algorithm. Finally, FRFs are calculated by using the ratio of the calculated responses and the excitation signal in the frequency domain. A representative FRF of the structure is shown in Fig.4.8 and it can be observed that the numerical FRF agrees quite well with the experimental one. Other selected points are also verified to assure that simulation algorithm works accurate, thus, numerical model is valid and can be used for a VRP study.
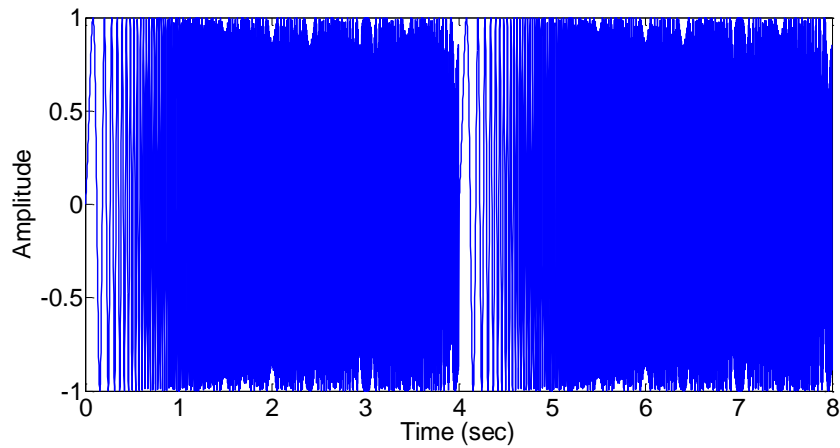
Figure 4.7 Sine-sweep signal
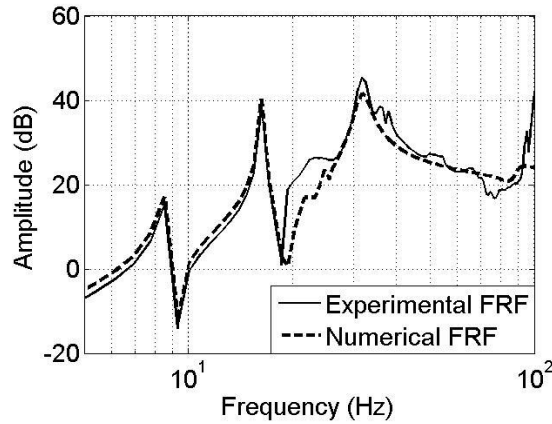
Figure 4.8 A representative FRF of the set-up

4.2.2   Selection of the Force Identification Points

Another consideration for hybrid VRP is the condition number of accelerance matrix to be inverted. Thus, numerical simulations are carried out to select the points where the force is to be identified according to the combined condition number. 17 candidate points are defined, as presented in Fig.4.9 and the accelerance matrix, $[H_{ij}(\omega)]$, is created for each set of two candidate points. Total of 136 combinations are considered. Combined condition numbers, calculated for each combination, are shown in Fig.4.10. According to the figure, out of 136 combinations, the best and worst combinations are determined as 5-8 and 13-16, respectively. The condition numbers of the accelerance matrices formed by these combinations are given in Fig.4.11 as a function of frequency. As seen in the figure, the condition numbers are reduced considerably when the accelerance matrix is created by the best combination.
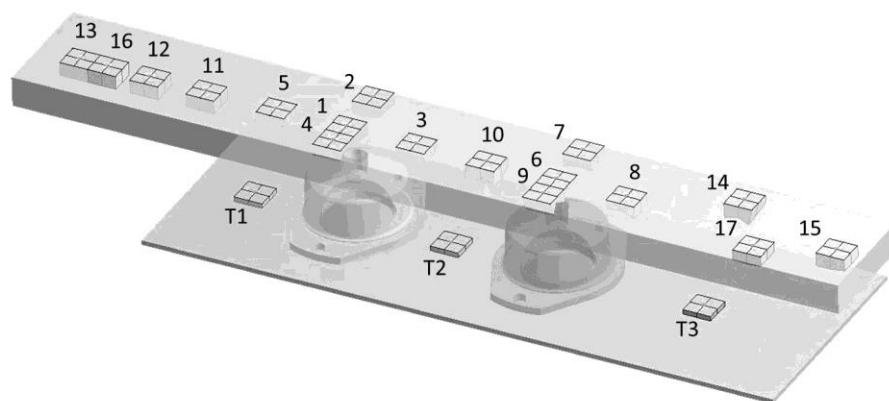
Figure 4.9 Candidate force identification points
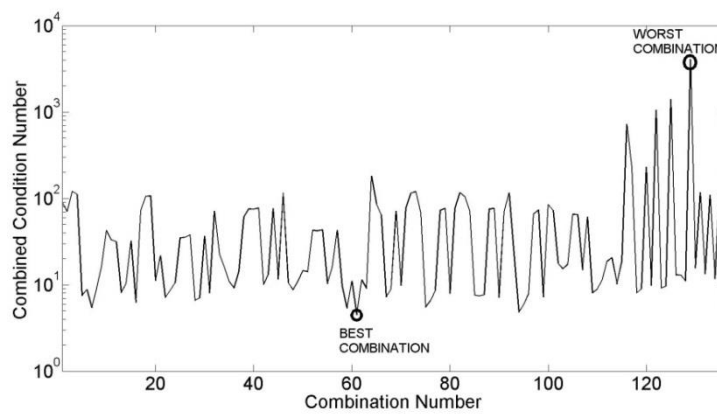
Figure 4.10 Combined condition number for each combination of two points
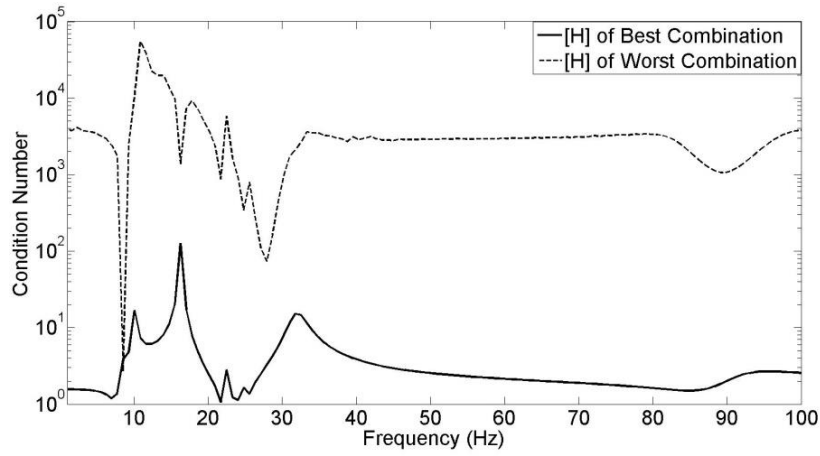
Figure 4.11 Condition numbers of best and worst combinations

4.2.3   Experimental and Hybrid VRP Results

After selecting the measurement points, the vibration response of the targets on the structure, shown in Fig.4.4, are predicted by implementing VRP methodology. The internal forces acting on the rubber mounts are identified by implementing Eq.(4.4). As shown in the equation, FRFs between point 5 and 8 are used to form the accelerance matrix.

$$\begin{Bmatrix} F_1(\omega) \\ F_2(\omega) \end{Bmatrix} = \begin{bmatrix} H_{55}(\omega) & H_{58}(\omega) \\ H_{85}(\omega) & H_{88}(\omega) \end{bmatrix}^{-1} \begin{Bmatrix} \ddot{X}_5(\omega) \\ \ddot{X}_8(\omega) \end{Bmatrix} \tag{4.4}$$

Once the forces acting on path inputs are identified, the responses of T1 and T2 are predicted by Eq.(4.2). Predicted responses of T1 and T2 points by hybrid VRP with the best and worst combinations are compared with the experimentally measured ones in Fig.4.12.(a) and (b). All of these results are also compared with the responses predicted by the experimental VRP where all required operational responses and FRFs are obtained experimentally for validation purposes.

The condition number of the numerical accelerance matrix is considerably lower than that of the experimental accelerance matrix, as seen in Fig.4.13. Due to the reduction in the condition numbers, it is seen that hybrid VRP method with the best combination improves the results significantly. Note that, a similar behavior is also observed for the other measurement location, T3. It can be observed that the combined condition number is an efficient guide for selecting the force identification points. However, it is observed that there are some discrepancies at specific frequencies for both methods. These discrepancies may have occurred due to the unconsidered in-plane lateral forces, rotations and moments.
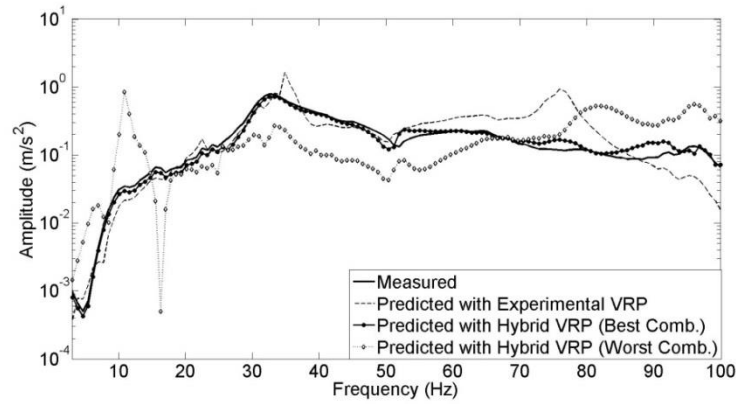
(a)
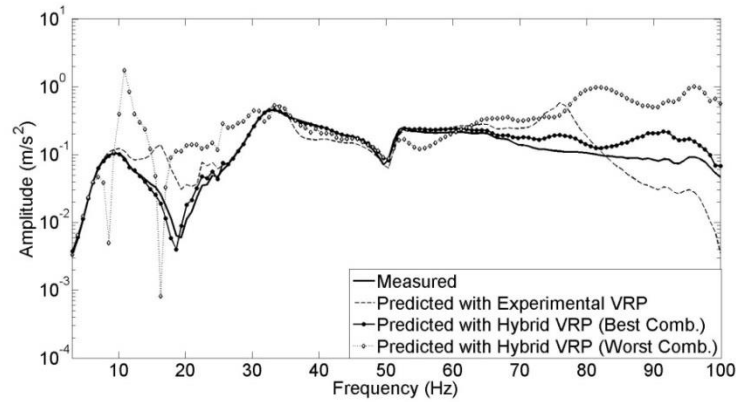
(b)

Figure 4.12 Predicted acceleration responses: (a) Sensor T1 (b) Sensor T2
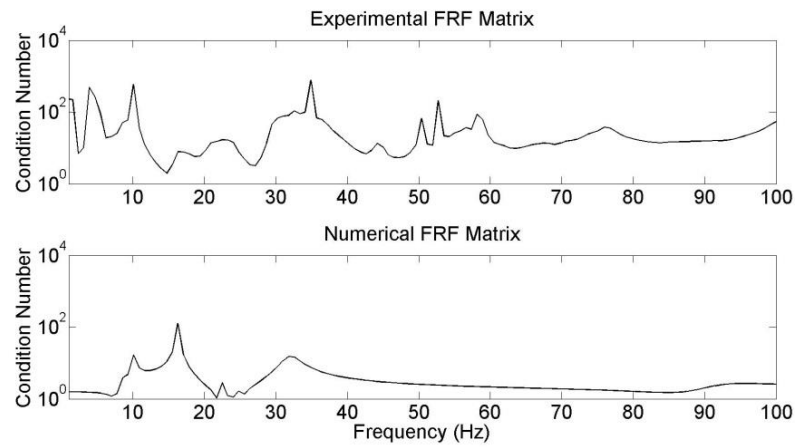
Figure 4.13 Condition numbers of experimental and numerical accelerance matrices

4.2.4   Effect of Shore Hardness

In this section of the study, the effect of shore hardness on the operational response prediction is investigated by using the simulation model introduced in Section 4.2.1. The same numerical set-up is used with different pair of mounts having shore hardness 45, 60 and 75 A, respectively. Numerical VRP studies are performed for each pair of rubber mounts having different shore hardness values. According to the results, the standard errors in predicting the vibration responses at the passive side are calculated and shown in Fig.4.14. Standard error is calculated by using standard deviation of the absolute error.
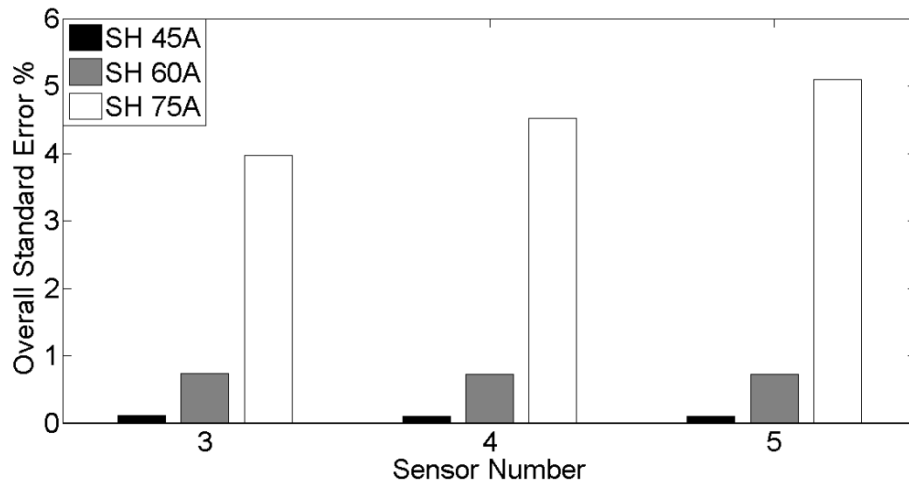
Figure 4.14 Overall standard error

It can be clearly observed in Fig.4.14 that the prediction error increases with increasing shore hardness of rubber. This observation is a result of linear relationship between the points at the active side. As explained above, VRP based on matrix direct inversion method, depends on the vibration response and FRF measurements at the active side. FRFs calculated between force identification points constitute the FRF matrix and the condition number of the FRF matrix is of great consideration. Higher condition number implies that the rows or columns of the FRF matrix are linearly dependent. Therefore, the relationship between the force identification points is essential. Averaged condition numbers of the FRF matrix with respect to different rubber mounts through the whole frequency of interest is tabulated in Table 4.1. It is observed that when harder rubber mounts are used, force identification points are getting linearly related to each other and exhibit similar responses. Therefore, the condition number increases and so the prediction error does.

Table 4.1 Average condition number of FRF matrix with respect to rubber hardness

	Average condition number of FRF matrix
Sh 45 A	3.51
Sh 60 A	3.85
Sh 75 A	4.47

4.3 Summary and Conclusions:

A hybrid vibration response prediction method based on the direct matrix inversion method is proposed for rubber linked structures with numerical and experimental case studies. FRF measurements were obtained numerically and vibration responses were measured experimentally in the proposed method. For this reason, a numerical model of the structure was created which also represent hyperelastic and viscoelastic behavior of the rubber mounts and validated by comparing calculated FRFs with the measured ones. In this study, it is also demonstrated that the point selection for force identification plays an important role in determining the condition number of the accelerance matrix. The force identification point selection is based on a metric that is composed of average condition number of the FRF matrix across the whole frequency of interest. The results show that the proposed hybrid methodology is superior to other alternative methods whereas the predictions are only based on the numerical results or experimental measurements. Although the application of hybrid VRP method is demonstrated for coupled structures with rubber mounts, it can be used for structures having rigid connections. Consequently, hybrid method can be considered as a reliable and efficient tool to predict the operational responses especially for complex structures.

Another consideration, the effect of the hardness of the couplings is also discussed by performing a numerical case study with different shore hardness values. It is observed that

the condition number of the accelerance matrix is reduced when softer couplings are used. This is due to the linear relationship between the points at the active side.

Chapter 5.

CONCLUSIONS

5.1 Summary of Dissertation and Conclusions:

Complex structures are usually composed of various subsystems coupled by several rigid or elastic couplings. Prediction of the vibration response at these complex structures such as aerospace, marine and automotive vehicles is an important engineering issue in terms of design optimization and component selection.

Considering these needs, this dissertation presents the vibration response prediction (VRP) methodologies such as mount stiffness method, transmissibility matrix method, matrix pseudo and direct inversion methods for the structures coupled with rigid and elastic couplings. Among the presented VRP methodologies, most consideration is given to the matrix inversion methods which involve an inverted FRF matrix and a vector of vibration responses. In some cases measuring FRFs are almost impossible, even if possible, they may be prone to significant errors. Besides, the FRF matrix to be inverted may become ill-conditioned due to the one or few modes that dominate the dynamics of the structure. Considering these problems, a hybrid vibration response prediction methodology, in which the numerical modeling results are integrated with the experimental measured data, is proposed. Considerations of this method such as the generation of accurate numeric model and the selection of points at where the force is to be identified are discussed within the scope of combined condition number of the FRF matrix.

In accordance with the presented methodologies, experimental and numerical case studies are conducted. Vibrating structures with rigid connections are of primary interest since real and complex structures usually composed of rigidly coupled substructures. At first, a rigidly coupled planar structure is considered and VRP methodology based on the matrix pseudo inversion method is applied along with singular value decomposition (SVD). Tikhonov regularization with the cross validation functions is investigated for improving the prediction results. A comparison of cross validation functions, which are used for selecting the regularization parameter, is presented. It is shown that Moore-Penrose pseudo inversion method gives satisfactory prediction results with some discrepancies at specific frequencies where the condition number is high. Thus, it can be stated that the condition numbers serve as the parameters influencing the prediction errors. Tikhonov regularization technique with OCV and GCV is found to be robust in improving the prediction results in the case of rigidly coupled structures. On the other hand, SCV method is found to be ineffective. Considering all Tikhonov regularization results, it is seen that it does not improve the prediction results considerably when the condition number is low. As a consequence, pseudo inversion technique is proven to be reliable but its application requires huge effort as well as extensive time since the paths should be disassembled and a huge amount of FRF measurements are needed.

Secondly, direct inversion method is applied for a structure coupled with two rigid links considering the cross-coupling effects and a comparison metric between the pseudo and direct inversion methods is presented. Compared to pseudo inversion technique, this method is found to be less time consuming, less challenging and the real boundary conditions are present since no disassembling is required. Meanwhile, it is shown that including cross-coupling terms improves the results with a rate of about 10-12 % and the predicted responses agree well having some discrepancies occurred due to the measurement errors. Moreover, effects of the measurement errors such as mass loading and

existing noise on the prediction results are demonstrated. It is observed that mass loadings can affect the results with discrepancies between 20 and 30 dB in magnitude whereas the contamination of the FRF data with a degree of 5 % results in errors up to 6 dB.

Finally, the structures connected with the elastic mounts are discussed since vibratory sources are usually connected to the supporting structures via rubber mounts in order to reduce the structure-borne noise transmissibility. In order to perform the hybrid VRP methodology for the rubber linked structure, hyperelastic and viscoelastic behavior of the rubber mounts are incorporated within the numerical model and a simulation algorithm is developed. Considerations of this method such as the generation of an accurate numeric model and the selection of force identification points are also discussed. Force identification points are selected based on a metric that is composed of average condition number of the FRF matrix across the whole frequency of interest. The effectiveness of the proposed method is determined by means of comparing the results with the experimental VRP results. The results show that the presented selection metric is an effective tool for determining the measurement points and the proposed hybrid methodology is superior to other alternative methods whereas the predictions are only based on the numerical results or experimental measurements. Consequently, hybrid method can be considered as a reliable and efficient tool to predict the operational responses especially for complex structures.

Another consideration for the structures having rubber mounts, the effect of the rubber hardness is also discussed by performing a numerical case study with different shore hardness values. It is observed that the condition number of the accelerance matrix is reduced when softer couplings are used.

5.2 Future Research:

This dissertation answers many questions related to the vibration response prediction studies. However, following areas can be explored in future studies.

- Application of strain gauges instead of accelerometers is of interest since the strain gauges present less cross-coupling at the path inputs and besides, sensor effects are minimized. This may result in low condition number of the FRF matrix.

- Since FRF measurements are prone to significant errors, analytical methods for FRF estimates should be developed.

- Time domain response prediction becomes critical for the shock loading especially on the naval platforms. The use of impulse response functions and convolution integral for the time domain response prediction should be investigated.

BIBLIOGRAPHY

[1] Wang, X., 2010, "Rationale and history of vehicle noise and vibration refinement," Vehicle noise and vibration refinement, X. Wang, ed., CRC Press, Boca Raton, FL, USA.

[2] Berglund, B., Lindwall, T., and Schwela, D. H., 1999, "Guidelines for Community Noise," W. H. O. (WHO), ed.Geneva.

[3] Heylen W., L. S., Sas P., 1997, Modal analysis theory and testing, Department of Mechanical Engineering, University of Leuven, Leuven, Belgium.

[4] Ewins, D. J., 2000, Modal Testing: Theory, Practice and Application, Research Studies Press Ltd., Hertfordshire, UK.

[5] Maia N., S. J., 1997, Theoretical and Experimental Modal Analysis, Research Studies Press Ltd., Somerser, UK.

[6] Rodrigues, J. F. D., Lopes, H., de Melo, F. Q., and Simões, J. A., 2004, "Experimental modal analysis of a synthetic composite femur," Experimental Mechanics, 44(1), pp. 29-32.

[7] Mohanty, P., and Rixen, D. J., 2005, "Identifying mode shapes and modal frequencies by operational modal analysis in the presence of harmonic excitation," Experimental Mechanics, 45(3), pp. 213-220.

[8] Suzuki, Y., Fujii, Y., and Watari, A., 1978, "Reduction of interior car noise by using vector method," SAE Technical Papers.

[9] Roesems, D., "Analysis of structure borne noise transmission paths," Proc. 6th Int. Seminar on Modal Analysis.

[10] Desanghere, G., "Identification of external forces based on frequency response measurements," Proc. 8th Int. Seminar on Modal Analysis.

[11] Desanghere, G., "Source identification methods based on input/output transfer function measurements: coherence analysis, energy allocation," Proc. 8th Int. Seminar on Modal Analysis.

[12] Hosseini Fouladi, M., Nor, M. J. M., and Ariffin, A. K., 2009, "Spectral analysis methods for vehicle interior vibro-acoustics identification," Mechanical Systems and Signal Processing, 23(2), pp. 489-500.

[13] Gajdatsy, P., Janssens, K., Desmet, W., and Van der Auweraer, H., 2010, "Application of the transmissibility concept in transfer path analysis," Mechanical Systems and Signal Processing, 24(7), pp. 1963-1976.

[14] Janssens, M. H. A., Verheij, J. W., and Thompson, D. J., 1999, "The use of an equivalent forces method for the experimental quantification of structural sound transmission in ships," Journal of Sound and Vibration, 226(2), pp. 305-328.

[15] Janssens, K., Gajdasty, P., and Van der Auweraer, H., "Operational path analysis: a critical review," Proc. ISMA 2008 International Conference on Noise and Vibration Engineering.

[16] De Klerk, D., and Ossipov, A., 2010, "Operational transfer path analysis: Theory, guidelines and tire noise application," Mechanical Systems and Signal Processing, 24(7), pp. 1950-1962.

[17] De Sitter, G., Devriendt, C., Guillaume, P., and Pruyt, E., 2010, "Operational transfer path analysis," Mechanical Systems and Signal Processing, 24(2), pp. 416-431.

[18] Janssens, K., Gajdatsy, P., Gielen, L., Mas, P., Britte, L., Desmet, W., and Van der Auweraer, H., 2011, "OPAX: A new transfer path analysis method based on parametric load models," Mechanical Systems and Signal Processing, 25(4), pp. 1321-1338.

[19] Van der Auweraer H., Mas P., Dom S., Vecchio A., Janssens K., and P., V. d. P., 2007, "Transfer path analysis in the critical path of vehicle refinement: the role of fast, hybrid and operational path analysis," Proc. SAE Noise and Vibration Conference.

[20] Verheij, J. W., 1982, "Multipath Sound Transfer from Resiliently Mounted Shipboard Machinery," TNO, Delft, Netherlands.

[21] Magrans, F. X., 1981, "Method of measuring transmission paths," Journal of Sound and Vibration, 74(3), pp. 321-330.

[22] Ribeiro, A. M. R., Silva, J. M. M., and Maia, N. M. M., 2000, "On the generalisation of the transmissibility concept," Mechanical Systems and Signal Processing, 14(1), pp. 29-35.

[23] Maia, N. M. M., Silva, J. M. M., and Ribeiro, A. M. R., 2001, "The transmissibility concept in multi-degree-of-freedom systems," Mechanical Systems and Signal Processing, 15(1), pp. 129-137.

[24] Ribeiro, A. M. R., Fontul, M., Maia, N. M. M., and Silva, J. M. M., 2005, "Further developments on the transmissibility concept for multiple degree of freedom systems," Proceedings of the XIth International Conference on Vibration Engineering, Timisoara, Romania.

[25] Verheij, J. W., "Experimental procedures for quantifying sound paths to the interior of road vehicles," Proc. 2nd Int. Conference on Vehicle Comfort, pp. 483-491.

[26] Starkey, J., and Merril, G., 1989, "On the ill-conditioned nature of indirect force measurement techniques," Int. Journal of Analytical Experimental Modal Analysis, 4, p. 6.

[27] Freymann, R., and Stryczek, R., "Noise path analysis and optimization," Proc. Unikeller Conference.

[28] Van der Linden, P. J., and Floetke, H., "Comparing inverse force identification and the mount stiffness force identification methods for noise contribution analysis," Proc. International Conference on Modal Analysis Noise and Vibration Engineering, pp. 2971-2986.

[29] Mas, P., Sas, P., and Wyckaert, K., "Indirect force identification based upon impedance matrix inversion: a study on statistical and deterministical accuracy," Proc. 19th Int. Seminar on Modal Analysis.

[30] Fabunmi, J. A., 1986, "Effects of structural modes on vibratory force determination by the pseudoinverse technique," AIAA Journal, 24(3), pp. 504-509.

[31] Thite, A. N., and Thompson, D. J., 2006, "Selection of response measurement locations to improve inverse force determination," Applied Acoustics, 67(8), pp. 797-818.

[32] Thite, A. N., and Thompson, D. J., 2003, "The quantification of structure-borne transmission paths by inverse methods. Part 1: Improved singular value rejection methods," Journal of Sound and Vibration, 264(2), pp. 411-431.

[33] Thite, A. N., and Thompson, D. J., 2003, "The quantification of structure-borne transmission paths by inverse methods. Part 2: Use of regularization techniques," Journal of Sound and Vibration, 264(2), pp. 433-451.

[34] Hendrickx, W., "Accurate vehicle FRF measurements for indirect force determination based upon matrix inversio," Proc. 19th Int. Seminar on Modal Analysis, pp. 1037-1048.

[35] Choi, H. G., Thite, A. N., and Thompson, D. J., 2006, "A threshold for the use of Tikhonov regularization in inverse force determination," Applied Acoustics, 67(7), pp. 700-719.

[36] Hillary, B., 1983, "Indirect measurement of vibration exciting forces," PhD, Imperial College of Science Technology and Medicine, London, UK.

[37] Stevens, K., "Force identification problems-an overview," Proc. SEM, pp. 838-844.

[38] Hundhausen, R. J., Adams, D. E., and Derriso, M., 2007, "Impact Loads Identification in Standoff Metallic Thermal Protection System Panels," Journal of Intelligent Material Systems and Structures, 18(6), pp. 531-541.

[39] Dobson, B. J., and Rider, E., 1990, "A Review of the Indirect Calculation of Excitation Forces from Measured Structural Response Data," Proceedings of the Institution

of Mechanical Engineers, Part C: Journal of Mechanical Engineering Science, 204(2), pp. 69-75.

[40] Adams, R., and Doyle, J., 2002, "Multiple force identification for complex structures," Experimental Mechanics, 42(1), pp. 25-36.

[41] Maia, N. M. M., Lage, Y. E., and Neve, M. M., 2012, "Recent advances on force identification in structural dynamics," Advances in Vibration Engineering and Structural Dynamics, F. Beltran-Carbajal, ed.

[42] Plunt, J., 2005, "Finding and fixing vehicle NVH problems with transfer path analysis," Sound and Vibration, p. 5.

[43] Gajdatsy, P. A., 2011, "Advances transfer path analysis methods," PhD, Katholieke Universiteit Leuven, Belgium.

[44] Urgueira, A. P. V., Almeida, R. A. B., and Maia, N. M. M., 2011, "On the use of the transmissibility concept for the evaluation of frequency response functions," Mechanical Systems and Signal Processing, 25(3), pp. 940-951.

[45] Steenackers, G., Devriendt, C., and Guillaume, P., 2007, "On the use of transmissibility measurements for finite element model updating," Journal of Sound and Vibration, 303(3–5), pp. 707-722.

[46] Lage, Y. E., Maia, N. M. M., Neves, M. M., and Ribeiro, A. M. R., 2013, "Force identification using the concept of displacement transmissibility," Journal of Sound and Vibration, 332(7), pp. 1674-1686.

[47] Wenjie, L., and Ewins, D. J., "Transmissibility properties of MDOF systems " Proc. 16th International Modal Analysis Conference, pp. 847-854.

[48] Devriendt, C., and Guillaume, P., 2008, "Identification of modal parameters from transmissibility measurements," Journal of Sound and Vibration, 314(1–2), pp. 343-356.

[49] Tcherniak, D., and Schuhmacher, A. P., "Application of transmissibility matrix method to NVH source contribution analysis," Proc. 27th International Modal Analysis Conference.

[50] Gajdatsy, P., Janssens, K., Gielen, L., Mas, P., and Van der Auweraer, H., "Critical assesment of operational path analysis; effect of coupling between path inputs," Proc. Acoustics 08 Conference.

[51] Gajdatsy, P., Janssens, K., Gielen, L., Mas, P., and Van der Auweraer, H., "Critical assesment of operational path analysis; mathematical problems of transmissibility estimation," Proc. Acoustics 08 Conference.

[52] Knapen, P. L., 1999, "Transfer Path Analysis related to Booming, performed on a car," No. 99-018, 52233/99-0125, Eindhoven University of Technology, Eindhoven, Netherlands.

[53] Penrose, R., "A Generalized Inverse for Matrices," Proc. Cambridge Philosophical Society p. 7.

[54] Anderson, E., Bai, Z., and Dongarra, J., 1992, "Generalized QR factorization and its applications," Linear Algebra and its Applications, 162–164(0), pp. 243-271.

[55] Gentle, J. E., 1998, Numerical Linear Algebra for Applications in Statistics, Springer-Verlag, Berlin, Germany.

[56] Turing, A. M., 1948, "Rounding-off errors in matriz processes," The Quarterly Journal of Mechanics and Applied Mathematics, 1(1), pp. 287-308.

[57] Verheij, J. W., 1997, "Inverse and reciprocity methods for machinery noise source characterization and sound path quantification. Part 2: transmission paths," Int. Journal of Acoustics and Vibration, 2(3), p. 10.

[58] Verheij, J. W., 1997, "Inverse and reciprocity methods for machinery noise source characterization and sound path quantification. Part 1: Sources," Int. Journal of Acoustics and Vibration, 2(1), p. 10.

[59] Janssens, M. H. A., Verheij, J. W., and Loyau, T., 2002, "Experimental example of the pseudo-forces method used in characterisation of a structure-borne sound source," Applied Acoustics, 63(1), pp. 9-34.

[60] Tikhonov, A. N., and Arsenin, V. I. A., 1977, Solutions of ill-posed problems, Winston.

[61] Nelson, P. A., and Yoon, S. H., 2000, "Estimation of acoustic source strength by inverse methods: Part I, Conditioning of the inverse problem," Journal of Sound and Vibration, 233(4), pp. 639-664.

[62] Yoon, S. H., and Nelson, P. A., 2000, "Estimation of acoustic source strength by inverse methods: Part II, Experimental investigation of methods or choosing regularization parameters," Journal of Sound and Vibration, 233(4), pp. 665-701.

[63] Hashemi, S., and Hammond, J. K., 1996, "The interpretation of singular values in the inversion of minimum," Mechanical Systems and Signal Processing, 10(3), p. 16.

[64] Allen, D. M., 1974, "The Relationship between Variable Selection and Data Augmentation and a Method for Prediction," Technometrics, 16(1), pp. 125-127.

[65] Golub, G. H., Heath, M., and Wahba, G., 1979, "Generalized Cross-Validation as a Method for Choosing a Good Ridge Parameter," Technometrics, 21(2), pp. 215-223.

[66] Thite, A. N., 2002, "Inverse determination of structure-borne sound sources," PhD, University of Southampton.

[67] Mas P., Sas P., and K., W., "Indirect force identification based upon impedance matrix inversion: a study on statistical and deterministical accuracy," Proc. ISMA Conference.

[68] W. Biermayer, F. B., R. Höldrich, A. Sontacci, S. Brandl, W. Fliesser, 2007, "Sound Engineering based on Source Contributions and Transfer Path Results," Journal of Society of Automative Engineers of Japan.

[69] Thite, A. N., 2003, "Inverse Determination of Structure-borne Sound Sources," Ph.D., University of Southampton.

[70] Kriel, T. E. S., 2000, Assessment of Frequency Domain Force Identification Procedures, University of Pretoria.

[71] Janssens, M. H. A., and Verheij, J. W., 2000, "A pseudo-forces methodology to be used in characterization of structure-borne sound sources," Applied Acoustics, 61(3), pp. 285-308.

[72] Jacquelin, E., Bennani, A., and Hamelin, P., 2003, "Force reconstruction: analysis and regularization of a deconvolution problem," Journal of Sound and Vibration, 265(1), pp. 81-107.

[73] Janssens K., G. P., Van der Auweraer H., "Operational path analysis: a critical review,," Proc. ISMA 2008.

[74] Cakar, O., and Sanliturk, K. Y., 2005, "Elimination of transducer mass loading effects from frequency response functions," Mechanical Systems and Signal Processing, 19(1), pp. 87-104.

[75] Bi, S., Ren, J., Wang, W., and Zong, G., 2013, "Elimination of transducer mass loading effects in shaker modal testing," Mechanical Systems and Signal Processing, 38(2), pp. 265-275.

[76] Dossing, O., "Prediction of transducer mass-loading effects and identification of dynamic mass," Proc. 9th International Modal Analysis Conference, p. 6.

[77] Peres M.A., Bono R.W., and Avitabile P., "Effects of shaker, stinger and transducer mounting on the measured frequency response functions," Proc. ISMA 2012, p. 15.

[78] Melody, J. W., Neat, G. W., "Integrated Modeling Methodology Validation Using the Micro-Precision Interferometer Testbed," Proc. 35th IEEE Conference on Decision and Control, p. 5.

[79] Basdogan, I., Elias, L. M., Dekens, F., and Sievers, L., 2006, "Predicting the Optical Performance of the Space Interferometry Mission Using a Modeling, Testing, and Validation Methodology," Journal of Vibration and Acoustics, 129(2), pp. 148-157.

[80] Devore, J. L., 2011, Probability and Statistics for Engineering and Science, Brooks/Cole, Cengage Learning.

[81] Kochanczyk M.D., B. T. F., Taute K.M., Florin E.L., 2012, "Power Spectral Density Integration Analysis and Its Application to Large Bandwidth, High Precision Position Measurements," Proc. SPIE Optical Trapping and Optical Micromanipulation IX.

[82] Jimin He, and Fu, Z.-F., 2001, Modal Analysis, Butterworth-Heinemann, Woburn,MA,USA.

[83] Sjöberg, M., 2002, On dynamic properties of rubber isolators [Elektronisk resurs], Institutionen för farkostteknik.

[84] Lord, H. C., 1930, "Vibration dampening mounting."

[85] Gregory, M. J., 1985, "Dynamic properties of rubber in automotive engineering," Elastomerics, 117(11), p. 6.

[86] Harris, J. A., 1987, "Dynamic Testing under Nonsinusoidal Conditions and the Consequences of Nonlinearity for Service Performance," Rubber Chemistry and Technology, 60(5), pp. 870-887.

[87] Turner, D. M., Boast, D., and Marfell, M., 2000, "Changes in the behaviour of rubber components as a consequence of real road conditions," IMECHE Conference Proceedings; 33-42 European conference on vehicle noise and vibration p. 10.

[88] Yu, Y., Naganathan, N. G., and Dukkipati, R. V., 2001, "A literature review of automotive vehicle engine mounting systems," Mechanism and Machine Theory, 36(1), pp. 123-142.

[89] Biermayer, W., Brandl, F., Höldrich, R., Sontacci, A., Brandl, S., and Priebsch, H. H., "Efficent transfer path analysis for vehicle sound engineering," Proc. JSAE Annual Congress Proceedings.

[90] Özşahin, O., Özgüven, H. N., and Budak, E., 2010, "Analysis and compensation of mass loading effect of accelerometers on tool point FRF measurements for chatter stability predictions," International Journal of Machine Tools and Manufacture, 50(6), pp. 585-589.

[91] Dossing, O., "Prediction of transducer mass-loading effects and identification of dynamic mass," Proc. 9th Int. Modal Analysis Conference, p. 6.

[92] Peres, M. A., Bono, R. W., and Avitabile, P., "Effects of shaker, stinger and transducer mounting on the measured frequency response functions," Proc. Int. Seminar on Modal Analysis, p. 15.

[93] Tönshoff, H. K., and Ahlborn, D., 1993, "Sensor orientation errors in frequency response function measurements," Int. Journal of Analytical and Experimental Modal Analysis, 8(3), p. 9.

[94] Lin, T. R., Farag, N. H., and Pan, J., 2005, "Evaluation of frequency dependent rubber mount stiffness and damping by impact test," Applied Acoustics, 66(7), pp. 829-844.

[95] Vriend, N. M., and Kren, A. P., 2004, "Determination of the viscoelastic properties of elastomeric materials by the dynamic indentation method," Polymer Testing, 23(4), pp. 369-375.

[96] Lu Z.H., W. L. R., Hagiwara I., "Finite element simulation of the static characteristics of a vehicle rubber mount," Proc. Proceedings of the Institution of Mechanical Engineers, Part D: Journal of Automobile Engineering, pp. 965-973.

[97] Valente L., M. L., 2001, "Vergleich des Neohooke'schen und Mooney-Rivlin'schen Material models in der FEM Brechnung," Periodica Polytechnica Ser. Mech. Eng., 45(1), p. 7.

[98] Dikmen, E., and Basdogan, I., 2008, "Material characteristics of a vehicle door seal and its effect on vehicle vibrations," Vehicle System Dynamics, 46(11), p. 16.

[99] Ogden, R. W., 1997, Non-linear Elastic Deformations, Dover Publications.

[100] Heller, V., and Chaplin, J. R., "Dynamic mechanical analysis of rubber used in Anaconda testing," Proc. Proc. 9th European Wave and Tidal Energy Conference.

[101] Ogden, J., 2010, "The Non-linear Properties of Rubber," BS, University of Southampton, Southampton, UK.

[102] Yeoh, O. H., 1993, "Some Forms of the Strain Energy Function for Rubber," Rubber Chemistry and Technology, 66(5), p. 18.

[103] Rivlin, R. S., 1948, "Large elastic deformations of isotropic materials. IV. Further developments of the general theory," Philosophical Transactions of the Royal Society of London, Series A, Mathematical and Physical Sciences, 241, p. 19.

[104] Zhou, Z., 1991, "Creep and stress relaxation of an incompressible viscoelastic material of the rate type," International Journal of Solids and Structures, 28(5), pp. 617-630.

[105] Cortés, F., and Elejabarrieta, M. J., 2006, "Modelling viscoelastic materials whose storage modulus is constant with frequency," International Journal of Solids and Structures, 43(25–26), pp. 7721-7726.

[106] Haneczok, G., and Weller, M., 2004, "A fractional model of viscoelastic relaxation," Materials Science and Engineering: A, 370(1–2), pp. 209-212.

[107] Roylance, D., 2001, "Engineering Viscoelasticity," Massachusetts Institute of Technology, Cambridge, MA, USA, p. 37.

[108] Wikipedia, 2015, "Generalized Maxwell model."

[109] Brown, R., 2006, Physical testing of rubber, Springer US.

[110] Qualitest, 2015, "HPE-II series digital durometers," Qualitest.

[111] Brown, R., 1999, Handbook of polymer testing, CRC Press.

[112] Smooth-on, 2015, "Durometer shore hardness scale."

[113] Gent, A.N., "On the Relation Between Indentation Hardness and Young's Modulus," Proc. Transactions of the Institute of the Rubber Industry, pp. 46-57.

[114] Battermann, W., and Köhler, R., 1982, Elastomere Federung, elastische Lagerungen: Grundlagen ingenieurmässiger Berechnung und Konstruktion, Ernst.

[115] Marvalova, B., 2007, "Viscoelastic properties of filled rubber. Experimental observations and Material Modelling," Engineering Mechanics, 14, p. 9.

[116] Haupt, P., and Sedlan, K., 2001, "Viscoplasticity of elastomeric materials: experimental facts and constitutive modelling," Archive of Applied Mechanics, 71(2-3), pp. 89-109.

[117] Mottahedi, M., Dadalau, A., Hafla, A., and Verl, A., 2011, "Numerical Analysis of Relaxation Test Based on Prony Series Material Model," Integrated Systems, Design and Technology 2010, M. Fathi, A. Holland, F. Ansari, and C. Weber, eds., Springer Berlin Heidelberg, pp. 79-91.

APPENDIX A.

THEORY OF RUBBER AND RUBBER MODELING

A.1 Theory of Rubber

Rubber or elastomeric materials are widely used as vibration isolators having elastic and viscous properties such as high inherent damping, deflection capacity and energy storage. Among these characteristics, they are compact, easily available, cost effective and maintenance free. The dynamic properties of these components are of primary concern in designing rubber isolators to reduce transmissibility. In order to determine the dynamic properties of the rubber, mathematical models are created in terms of hyperelasticity and viscoelasticity. The hyperelastic and viscoelastic material models represent the nonlinear elastic and strain-rate dependencies of the overall rubber behavior, respectively. Hyperelastic material model captures the material's nonlinear elasticity with no-time dependence whereas viscoelastic model describes the material response which contains an elastic and viscous part depending on time, frequency and temperature.

Several studies have been conducted to characterize the rubber's mechanical properties. Lin et al. [94] presented a simple experimental method to evaluate the frequency dependent stiffness and damping characteristics of a rubber mount. This experimental method involves measuring complex FRF by an impact test and curve fitting the data obtained from the test. Kren and Vriend [95] used dynamic indentation tests in order to determine the viscoelastic properties of rubber components. The results were compared for rubbers with

different shore hardness and a semi-empirical relationship between hardness and the rigidity was derived. Lu et al. [96] conducted experiments with a rubber mount and developed a nonlinear finite element model (FEM) to investigate its large deformation behavior and compared the model and experimental results to validate their approach. Valente and Molnar [97] compared Mooney–Rivlin and Neo–Hooken hyperelastic material models for silicone rubber using Marc Mentat FEM software. Dikmen and Basdogan investigated the material properties of a rubber vehicle door seal by means of experimental and numerical studies [98].

A.1.1 Hyperelastic Constitutive Model

Hyperelasticity refers to materials which can exhibit large elastic strain that is recoverable. Most elastomers such as rubber and many polymer materials are categorized in this category. A hyperelastic material is still an elastic material which means that the material returns to its original shape once the force is released. The difference is that for a hyperelastic material, the stress-strain relationship is related to a strain energy density function, W and the model describes the nonlinear relationship between the stress and strain, as stated in Eq.(A.1) [99].

$$\sigma = \frac{\partial W}{\partial \varepsilon} \tag{A.1}$$

The strain occurred on a deformed rubber material is defined as;

$$\varepsilon_i[\%] = (\lambda_i - 1)100 \tag{A.2}$$

where λ_i is the stretch ratios with i=1, 2 and 3. The stretch ratio is basically the ratio of deformed length to initial length in three directions *(x, y, z).*

Strain invariants are basically used to measure the strains which are independent of the coordinate system used to measure the strains [98]. Thus, the following three strain invariants include the three stretch ratios.

$$I_1 = \lambda_1^2 + \lambda_2^2 + \lambda_3^2 \quad I_2 = \lambda_1^2 \lambda_2^2 + \lambda_2^2 \lambda_3^2 + \lambda_3^2 \lambda_1^2 \qquad I_3 = \lambda_1^2 \lambda_2^2 \lambda_3^2 \tag{A.3}$$

Rubber materials can be approximated as incompressible with $\lambda_1 \lambda_2 \lambda_3 = 1$ resulting in $I_3 = 1$ [100]. The strain energy density function can be defined in terms of strain invariants and stretch ratios. Volumetric and deviatoric terms of the strain energy density function for incompressible materials can be written as;

$$W = W_d(\bar{I}_1, \bar{I}_2) + W_b(J) \tag{A.4}$$

where J is the ratio of the final volume to the initial volume. Since the rubber is assumed to be incompressible, meaning that the Poisson's ratio is very close to 0.5, no additional volumetric test is performed. Thus, it is considered that the energy stored in a volume of isotropic material is equal to the work done by the deformations expressed by $\lambda_1, \lambda_2, \lambda_3$. As for the deviatoric part, the equation for the stress of an incompressible material based on W is written as;

$$\sigma_1 = 2\left[\lambda_1^2\left(\frac{\partial W}{\partial I_1}\right) - \left(\frac{1}{\lambda_1^2}\right)\left(\frac{\partial W}{\partial I_2}\right)\right] + p \tag{A.5}$$

where p is a hydrostatic pressure [101]. Several mathematical models for W are proposed for the analytical and numerical prediction of stress-strain behavior of elastomer materials where the most prominent may be Neo-Hookean, Mooney-Rivlin and Yeoh models [101-103]. All these models are semi-empirical and require experimental parameters from shear, uniaxial or biaxial tests. In this study, Neo-Hookean, Mooney-Rivlin and Yeoh models were considered and corresponding mathematical models are shown in Table A.1.

Table A.1 Constitutive hyperelastic material models

Hyperelastic Model	Strain Energy Density Function
Neo-Hookean	$W = C_{10} (I_1 - 3)$
Mooney-Rivlin	$W = C_{10} (I_1 - 3) + C_{01} (I_2 - 3)$
Yeoh	$W = C_{10} (I_1 - 3) + C_{20} (I_1 - 3)^2 + C_{30} (I_1 - 3)^3$

A.1.2 Viscoelastic Rheological Model

As discussed before, hyperelastic model represents the nonlinear elastic response with no time dependence. In order to model the time dependency of the rubber behavior, a viscoelastic rheological model must be employed. Two major types of experiments can be performed for viscoelastic modeling; transient and dynamic. In dynamic experiments, so called dynamic mechanical analysis (DMA), the stress or strain is varied sinusoidally with time and the response is measured at various different frequencies [100]. On the other hand, transient experiments involve deforming the material by simple elongation and following the response with time. These experiments are mainly composed of creep and relaxation tests. In a creep test, the stress is held constant and the strain increases with time whereas in a relaxation test, the strain is held constant and the stress decreases with time [104-106]. One of the basic rheological viscoelastic models which can anticipate relaxation behavior is Maxwell model which includes both elastic and viscous property of the material and consists of a linear ideally viscous Newtonian dashpot and linear elastic Hookean spring in series, as shown in Fig.A.1. This model can anticipate relaxation behavior and is usually applied for the small deformations [104, 105]. Since the elements are connected to each other in series, the stress on each element is the same and equal to the imposed stress, while the total strain is the sum of the strain, as stated in Eq.(A.6).
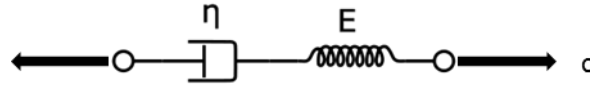
Figure A.1 Maxwell model

$$\sigma = \sigma_s = \sigma_d; \quad \varepsilon = \varepsilon_s + \varepsilon_d \tag{A.6}$$

where the subscripts *s* and *d* is denoted for the spring and dashpot, respectively. In a stress relaxation test since the strain is held constant, strain rate should be zero [107]. Taking the derivative of strain with respect to time;

$$\frac{d\varepsilon}{dt} = \frac{d\sigma}{dt}\frac{1}{E_s} + \frac{\sigma}{\eta_d} = 0 \tag{A.7}$$

Integrating Eq.(A.7), the stress is obtained as a function of time.

$$\sigma(t) = \sigma_0 \exp\left(-\frac{t}{\tau}\right); \quad \tau = \frac{\eta_d}{E_s} \tag{A.8}$$

where σ_0 is the initial stress and τ is the relaxation time. As stated in Eq.(A.8), the stress decays exponentially with time when the strain is held constant.

Advanced form of this model, which is called Generalized Maxwell Model, takes into account that relaxation does not take place at a single time but during a series of times. Thus, it has many spring-dashpot Maxwell elements as shown in Fig.A.2.
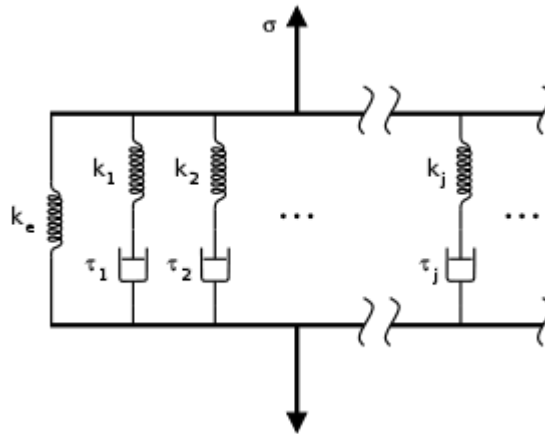
Figure A.2 Generalized Maxwell model [108]

Prony series is one of the best functions for modeling the linear viscoelasticity and generalized Maxwell model. The resulting stress vs. time data from a tensile relaxation test can be fitted with Prony series as seen in Eq.(A.9).

$$E(t) = E_\infty + \sum_{i=1}^{N} E_i \exp\left(-\frac{t}{\tau_i}\right) \tag{A.9}$$

where E_∞ is the long-term modulus and N is a finite integer. The instantaneous modulus is given by $E(t=0)$.

A.1.3 Shore Hardness

Hardness is a measure of an elastomer's response to a small surface stress. In the 1920s Albert F. Shore defined a hardness scale and developed a measurement device, called durometer, to measure the shore hardness of the elastomers, as shown in Fig.A.3. The term durometer is often used for the measurement as well as the instrument itself [109].


Figure A.3 Digital durometer [110]

Shore hardness is an indirect measure of Young's modulus and related moduli of an elastomeric or rubber material [111]. As a property of rubber, modulus is the ratio of stress and strain at some loading condition which is similar to the same property of metals.

However, unlike metals having a linear stress-strain relationship below the yielding point, rubber poses non-linear stress-strain relationship over a range of loading conditions. Stress-strain curve for the rubber can be considerably influenced by the ambient temperature, as mentioned before. Accordingly, the modulus of a rubber depends on the measurement conditions. These properties play an important role in the performance of rubber vibration and shock isolators.

Durometer measures the resistance to the penetration of an indenter point into the surface of a molded elastomer specimen. Higher durometer indicates harder rubber compound. Softer compounds stretch more and fasten better on rough surfaces compared to harder ones. Moreover, softer rubber materials creeps more and have a lower tensile strength than that of harder material. On the other hand, harder compounds pose greater abrasion resistance and resistance to extrusion. Consequently, rubber shore hardness is an important property and should be properly selected according to the application. The shore hardness scales and some of the applications are given in Fig.A.4. Rubbers used in vibration and shock isolators generally fall in the range of 35-75 durometer on the Shore A scale.
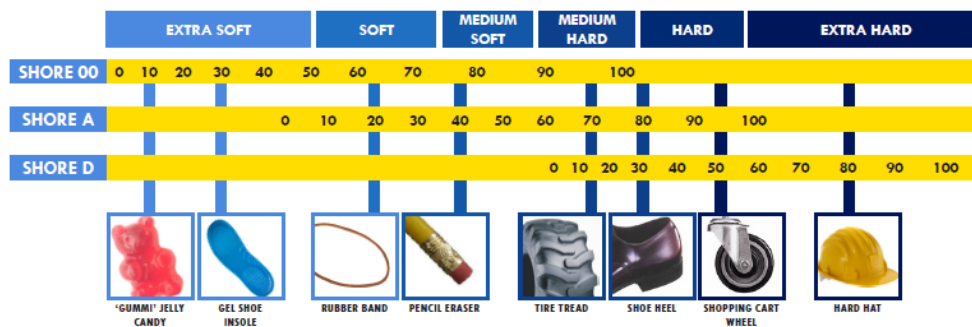
Figure A.4 Shore hardness scales [112]

Since shore hardness is an indirect measure of the stiffness, it can be directly related to Young's Modulus. One of the study on this relationship was performed by Gent [113]. He derived a semi-empirical equation, as follows;

$$E = \frac{0.0981\,(56 + 7.62336\,S)}{0.137505\,(254 - 2.54S)} \tag{A.10}$$

where S is the shore hardness and E is the Young's modulus. Ideally the hardness scale should convert a modulus range of $0 \rightarrow \infty$ to a hardness scale of $0 \rightarrow 100$. Eq.(A.10) executes this for S=100 but not for S=0. There are small departures from the master curve at S values below 40 given in Gent's paper. Another relationship between type A shore hardness and elastic modulus, E is given by Rigbi.

$$S = 35.22735 + 18.75487\,\ln(E) \tag{A.11}$$

Battermann and Köhler [114] derived an empirical formula which defines the relationship between the shear modulus, G and the shore hardness.

$$G = 0.086\,(1.045^{S}) \tag{A.12}$$

A.2 Rubber Components Modeling

The rubber mounts used in the case study is made of natural rubber with different shore hardness values, 45, 60 and 75 A. In order to evaluate the dynamic properties of the rubber, uniaxial tensile and relaxation test are conducted on the specimens created according to DIN 53504-S1 with a thickness of 2 mm as seen in Fig.A.5. For each type of rubber, identical three specimens are used for all specified tests. Universal tensile test machine used for the tensile and relaxation tests is shown in Fig.A.6.

|	A	B	C	D	G	R1	R2
DIN 53504 (mm)	115	25	33	6	25	14	25
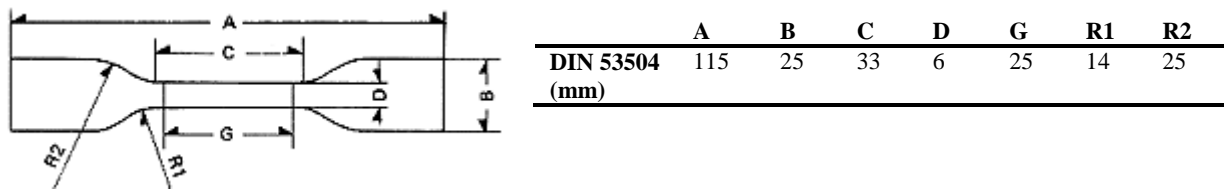
Figure A.5 Rubber specimen

Figure A.6 Universal tensile test machine

All tests are performed at constant room temperature under strain control. To study the hyperelastic properties, specimens are subjected to quasi static uniaxial tensile loading with constant 25 mm/min strain rate and three cycle of experiment was conducted to minimize the experimental errors. Fig.A.7 presents the stress-strain responses as obtained from the quasi static test and estimated coefficients of hyperelastic models for shore 75 A natural rubber are tabulated in Table A.2.
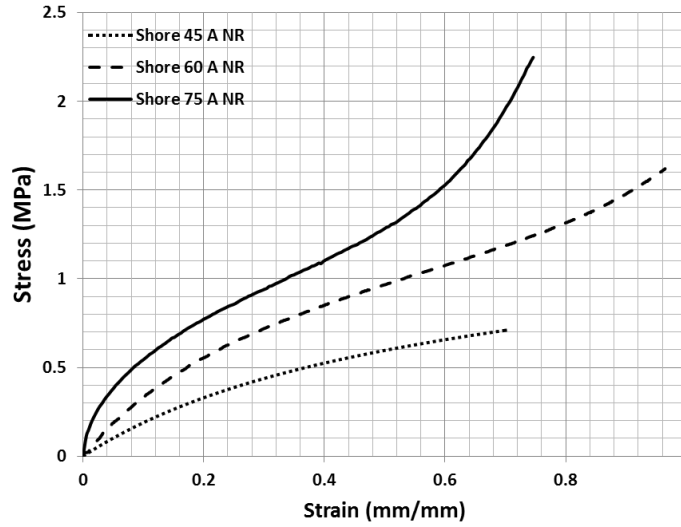
Figure A.7 Stress-strain responses from uniaxial tensile test

Table A.2 Estimated hyperelastic coefficients of shore 75 A natural rubber

Hyperelastic Model	C_{10}	C_{20}	C_{30}	C_{01}
Neo-Hookean	0.6933	-	-	-
Mooney-Rivlin	0.3724	-	-	0.4397
Yeoh	0.9636	-06213	0.3265	-

The relaxation behavior of the rubber specimens is examined through relaxation tests. Fig.A.8 shows the time histories of the stress decrement at a constant strain. Stress relaxation data, shown in the figure, is normalized to determine how the behavior of the specimen changes with increasing hardness. All curves initially reveal the existence of a very fast stress relaxation followed by a very slow rate of relaxation that continues in a asymptotic sense, as it is confirmed in [115, 116]. As it is also expected from a relaxation test, the shear modulus is decreasing with respect to time, or in other saying, the material resistance against the displacement is decreasing. This is due to the viscous effect existing in the dashpot of the rheological Maxwell model which eventually approaches to its

asymptote [117]. It is also noticeable that decreasing hardness results in faster relaxation. In this case study, generalized Maxwell model is used and Prony coefficients are determined by applying curve fitting to the relaxation test data. These coefficients are used as the viscoelastic model of the rubber.

<div align="center">(a)   (b)</div>
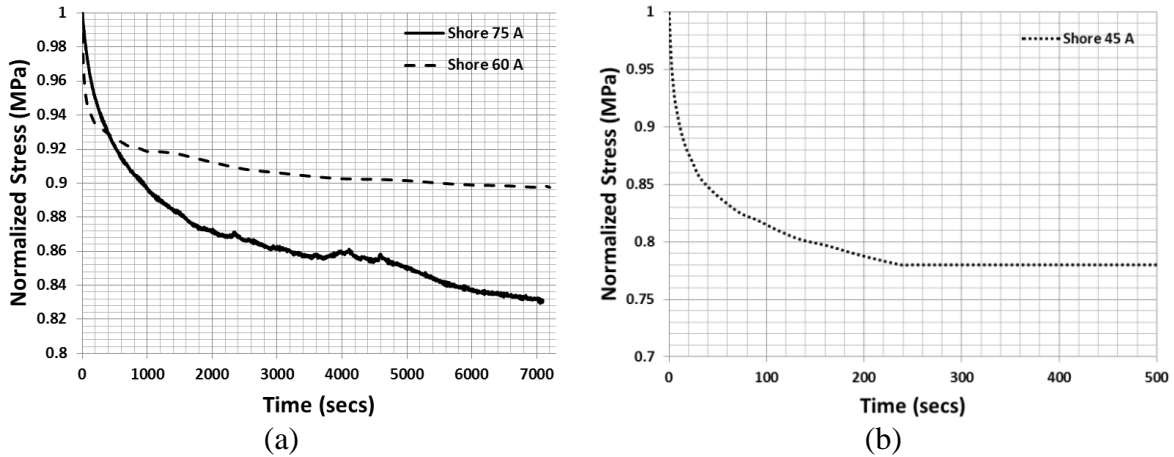
Figure A.8 Relaxation test results for; (a) Shore 75 A and Shore 60 A (b) Shore 45 A

In order to validate the experimentally obtained coefficients, a numerical simulation, based on finite element method (FEM), is performed. An identical specimen is created, as illustrated in Fig.A.9.(a), and the natural rubber with experimentally obtained material models is assigned as the material of the specimen to determine the best model. The specimen is constrained at one end and a ramp rising displacement at a constant velocity is applied on the other end. Reaction forces are calculated at the clamped bottom side of the specimen and summed to find out the engineering stress applied to the specimen centroid. The results are shown in Fig.A.9.(b) and (c). As shown from the numerical results, among three models, Yeoh shows the best agreement with the experimental data. As for the viscoelastic model, it can be stated that there is a good correlation between the Prony coefficients and the numerical results.
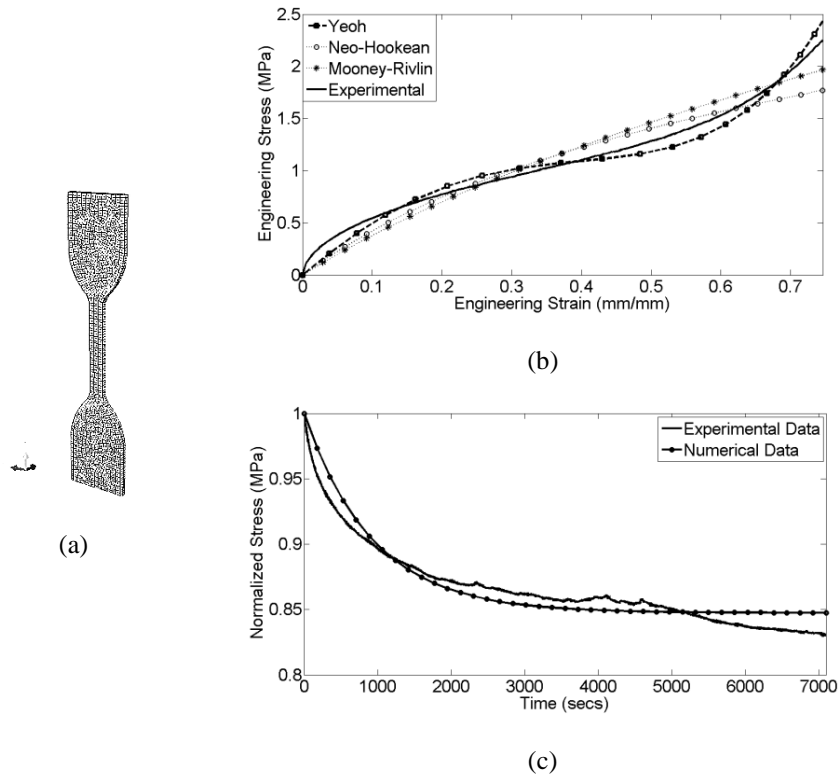
Figure A.9 Numerical simulation results for Shore 75 A natural rubber; (a) FEM model of specimen (b) Engineering stress-strain curve comparison (c) Relaxation curve comparison

The experimentally obtained data is also compared with Gent's relation and Rigbi formula which constitute a relationship between ASTM D2240 shore hardness and the Young's modulus. As seen in Fig.A.10, it is evident that the correspondence between the predicted value by Gent's relation and experimental value is more satisfactory compared to that of Rigbi formula.
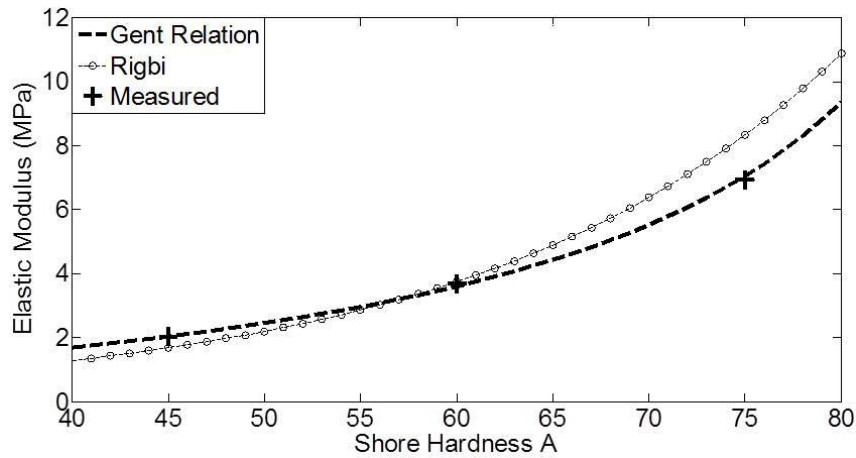
Figure A.10 Shore hardness vs elastic modulus

In addition, the measured shear modulus with respect to the shore hardness is also compared with the predicted values by Battermann-Köhler relation. According to Fig.A.11, it can be stated that initial shear modulus obtained by Yeoh model shows a good agreement with the Battermann-Köhler relation.
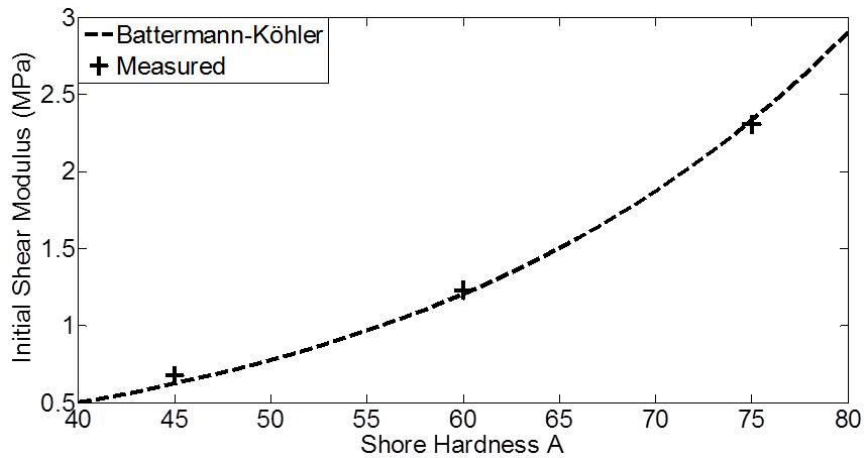
Figure A.11 Shore hardness vs shear modulus